DYNAMIC GEOMETRY AND PLAQUE DEVELOPMENT IN THE CORONARY ARTERIES

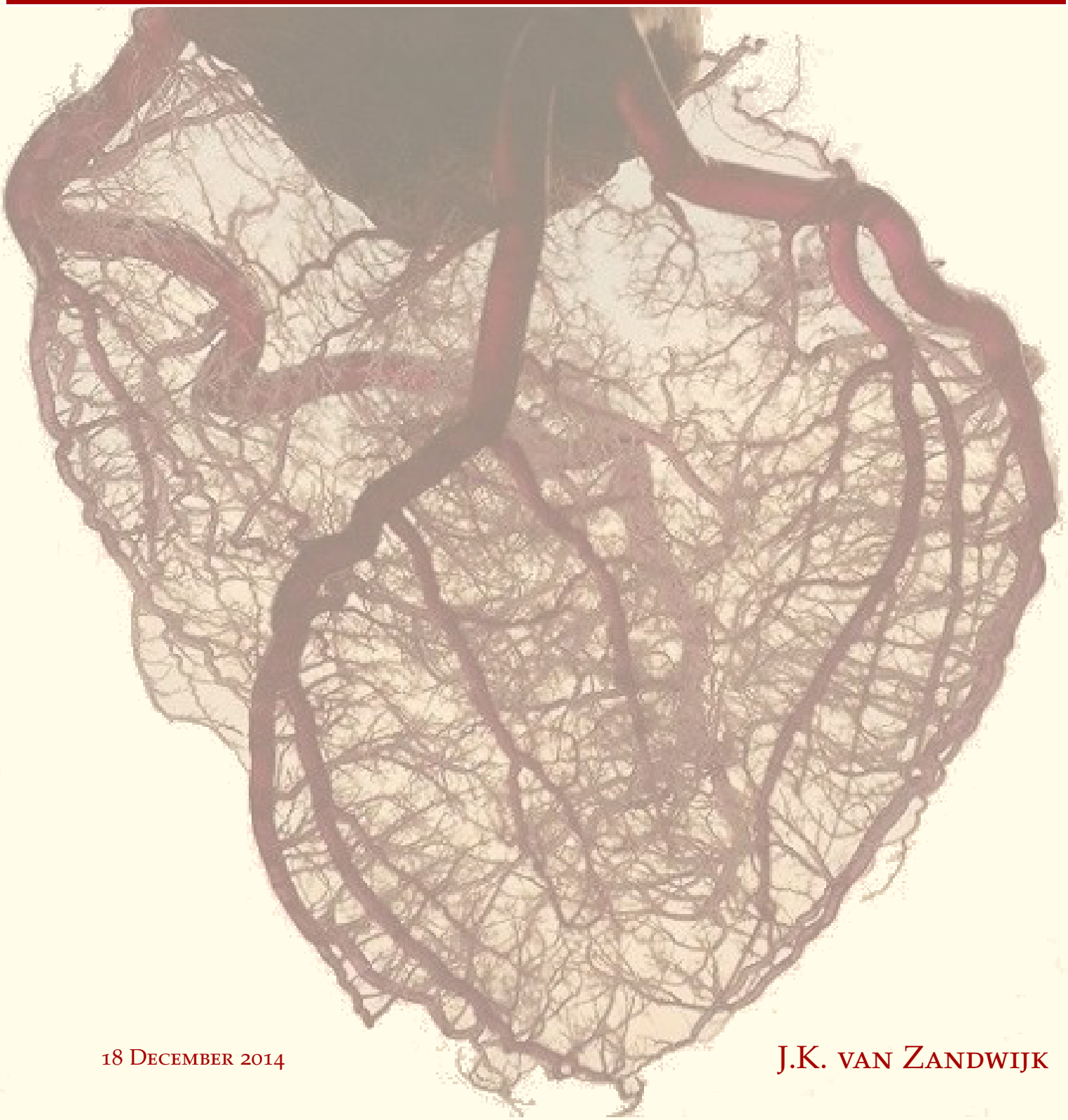

18 December 2014

J.K. van Zandwijk

Technical Medicine – Medical Imaging & Interventions
Faculty of Science and Technology, University of Twente

Department of Radiology & Center for Medical Imaging – North East Netherlands (CMI-NEN)
University of Groningen, University Medical Center Groningen

Cover photo credit: Rob Jones (http://www.flickr.com/photos/glockoma/398476805/)

MASTER'S THESIS

Dynamic Geometry and Plaque Development in the Coronary Arteries

– The potential of an innovative dynamic biomarker for coronary artery disease based on dual source computed tomography –

by

JORDY KRISTIAN VAN ZANDWIJK

Graduation committee

Technical supervisor & Chairman:	Prof. C.H. Slump, PhD
	Signals and System group, Department of EWI, University of Twente
Technical supervisor:	P.M.A. van Ooijen, PhD
	Department of Radiology, University Medical Center Groningen
	Center for Medical Imaging – North East Netherlands (CMI-NEN)
Medical supervisor:	R. Vliegenthart, MD, PhD
	Department of Radiology, University Medical Center Groningen
	Center for Medical Imaging – North East Netherlands (CMI-NEN)
Mentor:	P.A. van Katwijk, MSc
	Technical Medicine program, University of Twente
External member:	B.A. van Driel, MD
	Technical Medicine program, University of Twente
	MIRA institute for Biomedical Technology and Technical Medicine, University of Twente

Voorwoord

Beste lezer,

U leest nu mijn laatste werk van de opleiding Technische Geneeskunde (*bachelor*) – Technical Medicine (*master*), ook wel ***Master's Thesis*** genaamd. Van december 2013 tot december 2014 heb ik hieraan gewerkt bij de afdeling Radiologie van het Universitair Medisch Centrum Groningen. In deze periode heb ik mij verdiept in de wondere wereld van het hart, haar kransslagaderen, de eindeloze mogelijkheden om dit te visualiseren en hoe/of deze beeldvorming gebruikt kan worden om meer inzicht te krijgen in wie hartpatiënten worden en waarom. Een speerpunt hierin is het onderzoeken van het hart op een zo minimaal invasief mogelijke wijze: een algemene filosofie die de mastertrack 'Medical Imaging & Interventions' in mijn ogen belichaamt. In dit kader is het de kunst om met zo weinig mogelijk schade aan de patiënt, zo veel mogelijk informatie te verkrijgen, wat bij kan dragen aan meer therapeutische mogelijkheden of - in het huidige geval - een betere diagnostiek.

Tevens ben ik naast onderzoeker één dag in de week voornamelijk bij de afdeling Radiologie actief geweest op diverse subafdelingen om de laatste klinische ervaring in mijn opleiding op te doen. Enerzijds ben ik nauw betrokken geweest bij radiologische onderzoeken voor patiënten met (verdenking op) coronairlijden, en anderzijds heb ik inzichten en ervaring kunnen vergaren bij de secties interventieradiologie, neuroradiologie, abdomen radiologie (echografie), (interventie-)cardiologie, en thoraxchirurgie. Dit alles heeft mij gebracht naar waar ik nu sta: aan de drempel van een medisch-academische wereld met legio onontgonnen gebieden waar mijns inziens nog talloze technische innovaties kunnen worden ontdekt en toegepast om patiëntenzorg te verbeteren.

Ik hoop met dit werk te laten zien wat het nut kan zijn van het meten hoe kransslagaderen er geometrisch uitzien en hoe ze bewegen tijdens de hartcyclus, en dat de afdeling Radiologie/CMINEN hier potentie in ziet om zich verder te interesseren in dit onderwerp.

Jordy van Zandwijk

Groningen, 4 december 2014

Summary

Introduction: Development of atherosclerotic plaques in the coronary arteries is reported to be influenced and enhanced by hemodynamic deviating situations. Coronary hemodynamics could in turn be influenced by static and dynamic geometry of the coronary arteries. These relationships could be used as identifiers to determine coronary artery disease risk profiles. However, the evidence in this area is mainly based on invasive techniques such as intravascular ultrasound and therefore sparse, and not suitable to be applied in a screening environment or in asymptomatic patients.

Goals: To establish a method for quantifying coronary geometry characteristics in both static and dynamic situations, and to demonstrate relationships between coronary geometrical parameters and plaque development in the coronary arteries by using non-invasive imaging with computed tomography (CT).

Methods: All patients in this study underwent coronary CT angiography with high-resolution reconstructions in one phase (*patient Group 1*) or low-resolution reconstructions in multi-phases (*patient Group 2*) of the cardiac cycle. Group 1 involved patients with extra-cardial arterial disease, and Group 2 patients scheduled for elective coronary angiography. Three-dimensional reconstructions of centerlines through the major coronary arteries were obtained using commercially available software. End-diastolic phases, respectively end-diastolic and end-systolic phases were used in quantification of static (Group 1) and dynamic (Group 2) geometrical parameters. These parameters included vessel length, curvature, tortuosity, and the number of inflection points. Plaque development was assessed as degree of stenosis, plaque type and length, and the cross-sectional distribution of plaque. Associations between geometry and plaque development were statistically investigated.

Results: Static geometrical parameters showed an association with plaque development (patient Group 1, n=73). Dynamic geometrical parameters in patient Group 2 (n=71) could quantify changing geometry on artery and segment level in terms of curvature, tortuosity, and inflection points. No associations were found in patient Group 2 between change in geometry through the cardiac cycle and degree of stenosis. Both static and dynamic geometrical parameters were

associated with length of plaque on segment level in patient Group 2. Plaques were preferably distributed close to the myocardium and in the inner curve of segments.

Conclusion: Static parameters of the coronary arteries are associated with degree of stenosis in the coronary arteries, but this association was not found for change in geometry through the cardiac cycle. However, based on the results of both patient groups, it can be concluded that the relation of static and dynamic geometrical parameters with plaque length in segments can be an indication of the extent of coronary artery disease. New and deeper insights in anatomy, motion, and deformation of the coronary artery tree were obtained, which could eventually lead to development of novel image biomarkers to identify risk of coronary artery disease.

Contents

CHAPTER 1

General Introduction

1.1 CORONARY CIRCULATION

1.1.1 *Anatomy*

The heart is an essential organ in the human body and needs oxygen supply for proper functioning. Usually just after the aortic valve, the first side branches of the aorta (i.e. coronary arteries) that distribute oxygenated blood to the myocardium originate: the right coronary artery (RCA) and the left coronary artery (LCA). The course of these arteries follows the shape of the myocardium and they give off numerous side branches to distribute oxygenated blood to the entire myocardium. Figure 1.1 depicts an overview of the coronary arteries and their location in relation to the myocardium. The American Heart Association (AHA) reporting system from 1975 [1] is still the maintained standard for describing segment classification of the coronary arteries. Segments of interest in this study are numbered in Figure 1.2.

The RCA arises from the anterior sinus of Valsalva and runs between the right atrium and right ventricle to the inferior part of the intraventricular septum through the right atrioventricular (AV) groove. The acute marginal branch is the most prominent side branch and represents the beginning of the distal segment. After the distal segment, the RCA continues in the AV groove and gives of a branch to the AV node and in approximately 85% of the cases a posterior descending artery (PDA) (right-dominant system) to supply the inferior wall of the left ventricle and the inferior part of the septum. The left coronary artery arises as the left main (LM) artery from the left aortic sinus of Valsalva and divides almost immediately into a left anterior descending (LAD) artery and left circumflex (LCx) artery. The LAD runs anteriorly through the interventricular groove, giving off branches to the interventricular septum and continues to the

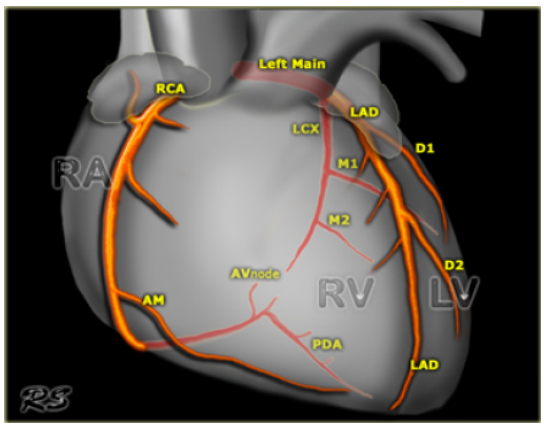

Figure 1.1 Anterior projection of the coronary arteries. The RCA, LAD, and LCx (see text for a description of their courses) are visible. From 'The Radiology Assistant'.

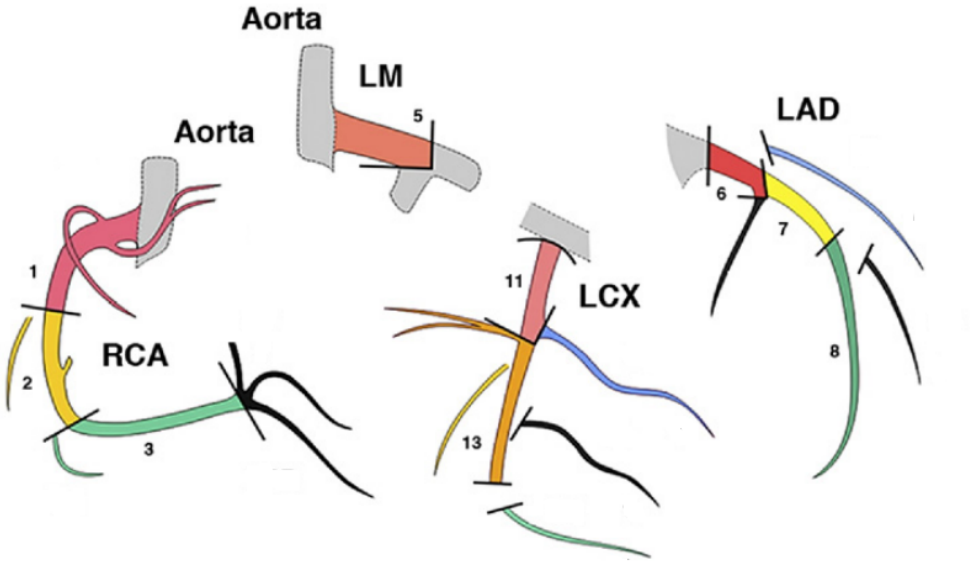

Figure 1.2 Schematic overview of the coronary artery segments. Relevant in this work are: 1 - proximal RCA, 2 - mid RCA, 3 - distal RCA, 5 - LM, 6 - proximal LAD, 7 - mid LAD, 8 - distal LAD, 11 - proximal LCx, and 13 - distal LCx. Adapted from [3].

apex of the heart. It supplies most of the left ventricle with its diagonal branches. The LCx in contrast, runs through the left AV groove to supply vessels for the lateral wall of the left ventricle. In most cases this artery is only marginally present and will end as an obtuse marginal branch, but in approximately 8% of the cases a PDA is supplied by the LCx (left-dominant system).[2]

1.1.2 *Coronary Artery Disease*

Coronary artery atherosclerosis has been the largest cause of death of humans in the Western civilization during the past decade.[4] Atherosclerotic changes in the walls of the coronary arteries are more commonly referred to as coronary artery disease (CAD). In this disease plaques are building up in the intimal and medial wall layers of the coronary arteries. Myocardial ischemia or infarction are life-threatening events that may occur due to lumen narrowing plaques or occluding blood clots at lesion sites. An example of atherosclerosis development is shown in Figure 1.3. Although patients with se-

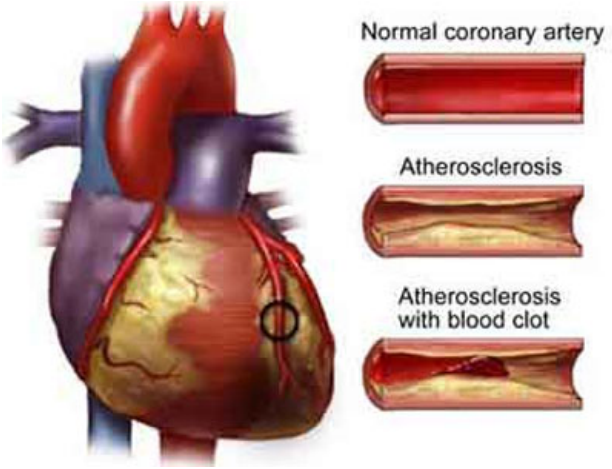

Figure 1.3 Examples a normal coronary artery, an artery with developed atherosclerosis, and with a jammed blood clot, resulting in complete obstruction of the artery at this point. Author: Tapan Chatterjee.

vere CAD develop signs and symptoms such as characteristic chest pain (angina) that are often easily identified, the disease can show no clinical signs during much of its development. The most serious risk for people with silent CAD is that sudden cardiac death (due to myocardial infarction) occurs before the first onset of symptoms.

A lot of research has addressed which patients will be (future) CAD patients and many risk factors have been revealed. These risk factors can provide reliable indications for physicians, but it is still difficult to predict in which particular patient atherosclerosis will develop and at which location. Some of these CAD risk factors can be controlled by lifestyle changes (e.g. smoking, lack of physical activity, unhealthy diet), whereas others can be controlled by patients less or not at all (e.g. high blood cholesterol, high blood pressure, diabetes). One proposed risk factor of CAD that cannot be controlled by patients is the specific geometry of the coronary arterial system, which could be a potential risk factor for (the onset of) atherosclerosis.[5] However, coronary arteries exhibit large variation in anatomic configuration and there are infinite methods of describing (or modeling) geometry. Some associations between preferred sites of CAD and geometry have been described,[6] but the added value of geometric information and whether it can be a potential risk factor are still subjects of debate.

1.1.3 *Imaging for CAD*

Hemodynamically significant stenoses in the coronary arterial system are causing ischemia of the myocardium supplied by the relevant vessel. The goal of coronary imaging is to provide a clinical tool that can reliably visualize the proximal, mid and distal coronary branches where hemodynamically significant stenoses could be present. Cardiac imaging in order to assess anatomical stenoses of the coronary arterial system is challenging in many aspects. For instance, cardiac motion and the small vessel size require adequate temporal and spatial resolution and

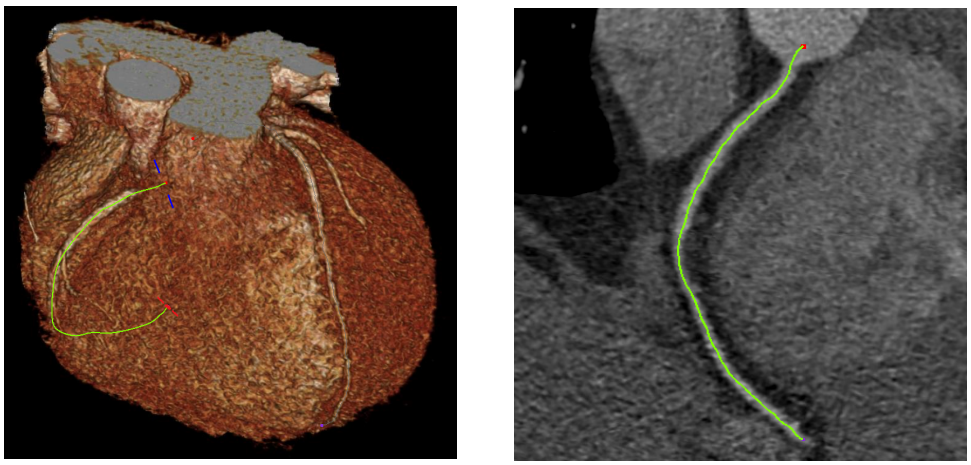

(a) 3D volume rendered image (RCA is green). **(b)** CPR view of the RCA in **(a)**.

Figure 1.4 Examples of visualization methods with a CT generated dataset. No atherosclerotic plaques are present in this RCA.

are therefore key elements in the choice of a suitable imaging modality.[7] The most accurate method for coronary imaging was until recently invasive coronary angiography (ICA), because of its superior temporal resolution over techniques as coronary computed tomography (CT) and magnetic resonance (MR) imaging.[8] Furthermore, its invasiveness allows physicians to perform revascularization techniques such as percutaneous coronary intervention or coronary stenting.[9] The main limiting factor of MR coronary imaging, is its lower spatial resolution which is required for adequate stenosis assessment.[8, 10]

Development of multi-detector computed tomography (MDCT) and dual-source computed tomography (DSCT) has led to improvements in both temporal and spatial resolution in CT imaging. This makes coronary computed tomography angiography (cCTA) the preferred choice for coronary assessment and the applied imaging modality throughout this study. An additional advantage over ICA is that CT can also provide information about the vessel wall and characterization of coronary plaques. The current imaging modality in University Medical Center Groningen (UMCG) is a 64-row dual-source CT scanner (Somatom Definition, Siemens Medical Systems, Erlangen, Germany). This first-generation DSCT scanner has a temporal resolution of 83 ms. Dedicated software allows users to apply multiple visualization techniques on the reconstructed data. Examples are the three-dimensional volume rendering technique (Figure 1.4a) and curved planar reformation (CPR) (Figure 1.4b and next paragraph). Study data was analyzed using Aquarius iNtuition (Ver.4.4.11, TeraRecon, San Mateo, USA)[1] commercially available software.

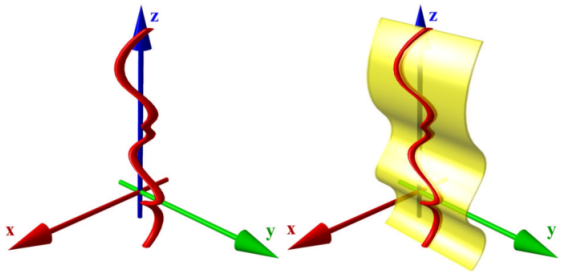

Figure 1.5 Visualization of the CPR principle. The red line represents a tubular structure (e.g. blood vessel). From [11].

CURVED PLANAR REFORMATION An important image reconstruction technique used in this work is CPR. In this process, tubular structures such as blood vessels are displayed along a longitudinal cross-section in order to assess morphology.[11] The central axis through the lumen is shown in the left side of Figure 1.5, with a re-sampled surface through the lumen on the right. Visualization of the structure with lumen is preserved. Objects that are on the curved surface and not touched by the centerline are reconstructed in a deformed manner. Distortion of objects in CPR is analogous to the mercator projection of the earth (see Figure A.1 and A.2 for this analogue example). Rotating the CPR around its central-axis is necessary to visualize and assess the entire lumen. A stretched CPR type is used, which has the main advantage of preserved voxel isometry, making length (and other centerline-based) measurements possible. CPR-based measurements were essential throughout this study.

[1] More information at http://www.terarecon.com/wordpress/our-solutions/intuition-workflow.

It is generally thought that deviations in blood flow play an important role in plaque development in the coronary arteries.[12] A parameter that is often used in describing hemodynamic alterations is wall shear stress (WSS), defined as the force per unit area that blood flow exerts on the vessel wall. WSS (τ_w) is dependent on blood viscosity and flow velocity profile, often simulated in computational fluid dynamics (CFD) studies as shown in Equation 1.1 (Newton's law of viscosity)[13].

$$\tau_w = \mu \left(\frac{\delta u}{\delta y} \right)_{y=0} \tag{1.1}$$

In this equation, μ is the dynamic viscosity of blood, u the velocity of the blood parallel to the vessel wall and y the distance to the vessel wall. The fraction $\frac{\delta u}{\delta y}$ represents the blood velocity gradient. Considering this equation, a major shortcoming of imaging techniques for accurate estimation of the WSS becomes clear as the inability of accurate arterial wall tracking. This needs to be performed with enough spatial and temporal resolution in the coronary arteries to provide a reliable quantification of τ_w.[13]

The WSS parameter has been found with CFD to be low in particular at bifurcations or at the inner curve of a blood vessel, of which an example can be seen by the dark blue color in Figure 1.6.[5] Furthermore, some studies use a time-averaged/oscillatory WSS as hemodynamic parameter, which has been associated before with early atherosclerosis.[14–16] Oscillatory WSS can be used for blood vessels that are non-moving (e.g. carotid/iliac arteries), but the coronary arteries are almost non-stop in motion. This life-time movement affects WSS parameters even more. Furthermore, evidence that plaque development occurs mostly at sites of low/oscillatory WSS is not always perfectly clear, and sufficient large study samples and studies considering human vessels instead of modeling them are required.[17]

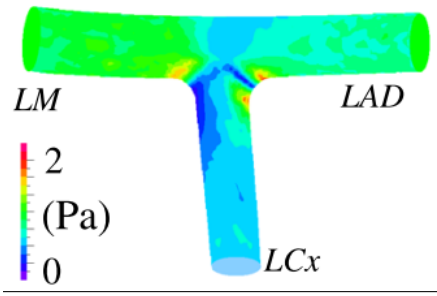

Figure 1.6 Example of the left coronary bifurcation with modeled WSS. Low WSS is especially seen at the inner curve of the LCx branching; a preferred site for atherosclerosis. Adapted from [5].

Hemodynamics have been associated before with specific geometry of the coronary arteries.[6, 18, 19] Furthermore, there are also studies that relate geometrical parameters such as vessel length, curvature, and tortuosity with the onset or presence of atherosclerosis.[5, 6, 16, 20] However, these (mostly CFD-based) studies are lacking geometrical information from real human coronary arteries in sufficient large numbers, or do not account for the change in geometry during the cardiac cycle. Another important rationale to use (dynamic) geometry as a potential biomarker for atherosclerosis, is that coronary geometry is thought to be affected less by atherosclerotic processes, in contrast to WSS.[6] The question arises whether dynamic coronary

geometry can be used as a biomarker or potential risk factor for atherosclerosis in the coronary arteries.

More rationale for investigating the influence or predictive value of geometrical characteristics of the coronary arteries on development of plaques, and substantiation from previous studies is given in the introduction sections of Chapter 2 and Chapter 3.

1.3 OBJECTIVES

Preliminary research at the Radiology department at University Medical Center Groningen was already initiated when this master internship started and conducted primarily by mr. V. Tuncay. This research focused on geometry assessments of the coronary arteries observed in a static situation. In this master internship, contributions were made to the already initiated research, and this was extended based on its observations, outcomes, and limitations. The primary aim of this study is to investigate how the coronary arteries are moving during the cardiac cycle and if there is a relationship with the development of atherosclerotic plaques in these arteries. The following main research questions were answered.

1.3.1 *Research Questions*

- What is the static relation between coronary geometry and the extent of CAD?
  ~ Chapter 2 (lead author V. Tuncay)
- How does coronary geometry change in different phases of the heart cycle?
  ~ Chapter 3
- What are the associations between sites of plaque development with specific dynamic coronary geometry?
  ~ Chapter 4

1.4 OUTLINE OF THIS THESIS

The purpose of the current chapter (**Chapter 1**) was to introduce the basics in this field of medicine, the applied techniques, and to get acquainted with relevant terminology. Furthermore, rationale for the initiation of this project was given to provide the reader background on research questions and setup.

The next chapter (**Chapter 2**) investigates the relation between the geometrical configuration of the coronary arteries in one phase of the cardiac cycle and the extent of CAD. This research was mainly performed by mr. V. Tuncay, on which the research from this thesis continues. His work is co-authored and the manuscript is therefore adapted and included as a chapter

in this thesis. **Chapter 3** proposes a more sophisticated quantification method of the changing coronary geometry during the cardiac cycle based on dynamic DSCT scans. This involves an other patient group than was used in Chapter 2. Using this method, differences were quantified with the available software. In **Chapter 4**, a more detailed method is established that describes the type, location, and severity of plaque development with respect to the hemodynamic basis of atherosclerotic processes in the coronary arteries. Subsequently, plaque quantifications will be associated with the geometrical difference results of Chapter 3, to provide insights about their interdependency or coherence.

Chapter 5 will finalize this thesis with specific attention to the geometrical parameters used in this work, and the potential to improve these parameters with respect to the hemodynamic relevance for the coronary arteries. Furthermore, directions for future research will be given, based on the findings and limitations that were discovered throughout this research. This thesis concludes with a general conclusion of the results from all chapters.

CHAPTER 2

Coronary Geometry and the Extent of Coronary Artery Disease

Manuscript title: CT angiography based coronary curvature and tortuosity in relation to the presence and extent of coronary artery disease

Authors: V Tuncay[1], R Vliegenthart[1,2], MAM den Dekker,[1,2], GJ de Jonge,[2], JK van Zandwijk[1,3], P van der Harst,[4], M Oudkerk,[1], ER van den Heuvel,[5], PMA van Ooijen,[1,2]

– Under preparation for submission –

2.1 INTRODUCTION

Atherosclerosis in the coronary arteries (coronary artery disease (CAD)) starts early in life and is the leading cause of mortality in the Western world.[4, 9] Plaques evolve over time and can cause narrowing of coronary arteries with consequently reduced coronary blood flow and cardiac ischemia. Coronary plaque rupture can lead to clot formation and complete acute occlusion of a vessel, with acute myocardial infarction as a consequence.

Development and progression of plaque is reported to be influenced by biochemical, biological, and mechanical factors.[21] One of the mechanical factors influencing the plaque process is shear stress on the coronary artery wall (i.e. WSS).[6, 21–23] In these *in vivo* studies, WSS was in turn dependent on the coronary artery geometry, with low shear stress being predominant in the inner curvature of the vessel. Atherosclerotic plaques are more often present at the inner curvature of the vessel, as well as at vessel bifurcations,[6, 20] although contradicting results have been reported.[24]

Gaining insight in the effect of the three-dimensional vessel geometry on plaque development could be of great importance to allow early detection of individuals at increased risk of CAD, and could serve as an additional predictive factor to be evaluated on anatomical imaging techniques. Therefore, we investigated the relationship between coronary curvature and tortuosity with presence and extent of CAD using non-invasive cCTA imaging.

[1] Center for Medical Imaging - North East Netherlands (CMI-NEN), University Medical Center Groningen
[2] Department of Radiology, University of Groningen, University Medical Center Groningen
[3] Technical Medicine Faculty, University of Twente
[4] Department of Cardiology, University of Groningen, University Medical Center Groningen
[5] Department of Epidemiology, University of Groningen, University Medical Center Groningen

2.2 METHODS

2.2.1 *Patients*

The current study is a sub-study of the GROUND-2 study, which evaluated the presence of coronary artery disease in asymptomatic patients with a history of extra-cardiac arterial disease.[25] All patients underwent non-invasive cardiac imaging by cCTA and adenosine perfusion MR imaging. The GROUND-2 study protocol was approved by the institutional review board of the UMCG, and written informed consent was obtained from all participants. Participants of the GROUND-2 study whose scans were reconstructed at end-diastolic (ED) phase were included in this sub-study. Patients filled out a questionnaire regarding extra-cardiac arterial disease, medical history, risk factors, medication use, and family history. Exclusions were made in cases of history or complaints of symptomatic CAD. Hypertension was defined as systolic blood pressure $\geq$140 mmHg and/or diastolic blood pressure $\geq$90 mmHg, or anti-hypertensive medication. Dyslipidemia was defined as LDL cholesterol $\geq$4.0 mmol/L, HDL cholesterol $\leq$1.2 mmol/L (women) or $\leq$1.0 mmol/L (men), triglycerides $\geq$4.0 mmol/L, or lipid-lowering medication. Diabetes was classified as fasting plasma glucose >7.0 mmol/L, known diabetes or medication for diabetes.

2.2.2 *Computed Tomography*

CT scans were performed on a dual-source CT scanner (SOMATOM Definition, Siemens, Erlangen, Germany) with a standardized scanning protocol. cCTA was performed in spiral mode, using retrospective electrocardiography (ECG)-gating. Pulsing window was dependent on heart rate. Below 65 beats per minute, data were acquired at 70-75% of the cardiac cycle, and above 65 beats per minute, a window of 35-75% was used. Patients received intravenous beta-blocker to lower the heart rate if necessary. All patients received nitroglycerin sublingually, for vasodilation. The following scan and reconstructions parameters were applied: 32x0.6 mm collimation, image acquisition 64x2x0.6 mm with flying z-spot, increment 0.4 mm, 330 ms rotation time, tube voltage and tube current according to body weight, pitch depending on heart rate of the patient, field-of-view 205 mm. Images were reconstructed as consecutive 0.6 mm slices.

2.2.3 *Assessment of Coronary Artery Disease*

Attending radiologists with experience in cardiac CT ranging from 5 to over 10 years performed analysis of the cCTA. Coronary evaluations were done on Syngo (Siemens, Erlangen, Germany). Severity of stenosis (significant/non-significant) was assessed for each major artery (RCA, LAD,

and LCx) and for each segment, according to the 15-segment modified AHA classification.[1] Significant stenosis was defined as ≥50% or ≥70% lumen surface reduction by visual assessment.

2.2.4 *Assessment of Coronary Artery Geometry*

Two observers independently performed coronary artery geometry assessment on the dedicated software (Aquarius iNtuition Ver.4.4.11, San Mateo, USA). Measurements were performed twice by the first observer (VT) for the whole data. The second observer (MdD) only performed measurements on a subset of 20 randomly selected datasets for inter-reader analysis. A standard cardiac workflow protocol was selected for the 3D reconstructions. Following automatic ribcage removal, related workflow steps were selected for detailed inspection of the main coronary arteries (RCA, LM, LAD, and LCx). The coronary arteries could be selected on the transverse slices or the volume rendered reconstruction (Figure 2.1), resulting in a CPR of the selected vessel with automated initiation of centerline extraction. Curvature and tortuosity measurements were performed based on the centerlines. Each segment was marked followed by semi-automated curvature and tortuosity measurements, which were performed on segment and artery level (Figure 2.2). Segments with an average diameter of less than 1.5 mm were not evaluated to ensure reproducibility. Arteries where centerline extraction was not possible were excluded. Curvature is basically defined as the inverse radius (Figure 2.3a) and is calculated with Menger's method.[26, 27] Average of the local curvatures on the range is given as the end result of the curvature measurement. Tortuosity is defined as the path length (P) of the centerline divided by the straight distance (D) between begin and endpoint (Figure 2.3b).[28]

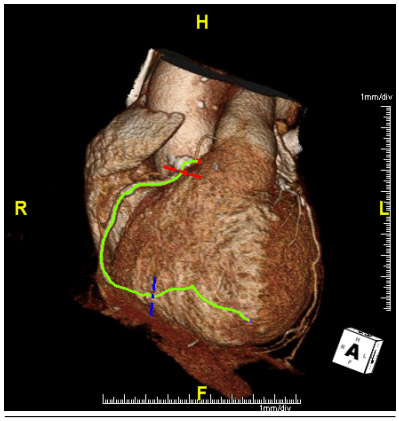

Figure 2.1 Volume rendered computed tomography image of an RCA centerline extraction.

2.2.5 *Statistical Analysis*

Statistical analyses were performed using SAS version 9.3 (SAS Institute Inc., Cary, NC, USA) and IBM SPSS Statistics version 20.0.0.1 (SPSS Inc., Chicago, IL, USA). The results of nonparametric descriptive statistics are given as median [25 and 75 percentiles]. Inter- and intra-reader agreement was determined and intraclass correlation coefficient (ICC)'s were calculated by the bivariate correlations analysis of SPSS to assess inter- and intra-reader agreement for curvature and tortuosity. The ICC can be interpreted as: 0-0.2 poor agreement; 0.3-0.4 fair agreement; 0.5-0.6 moderate agreement; 0.7-0.8 strong agreement and ICC >0.8 almost perfect agreement.[29] Intra- and inter-reader differences were assessed by Bland-Altman plots.

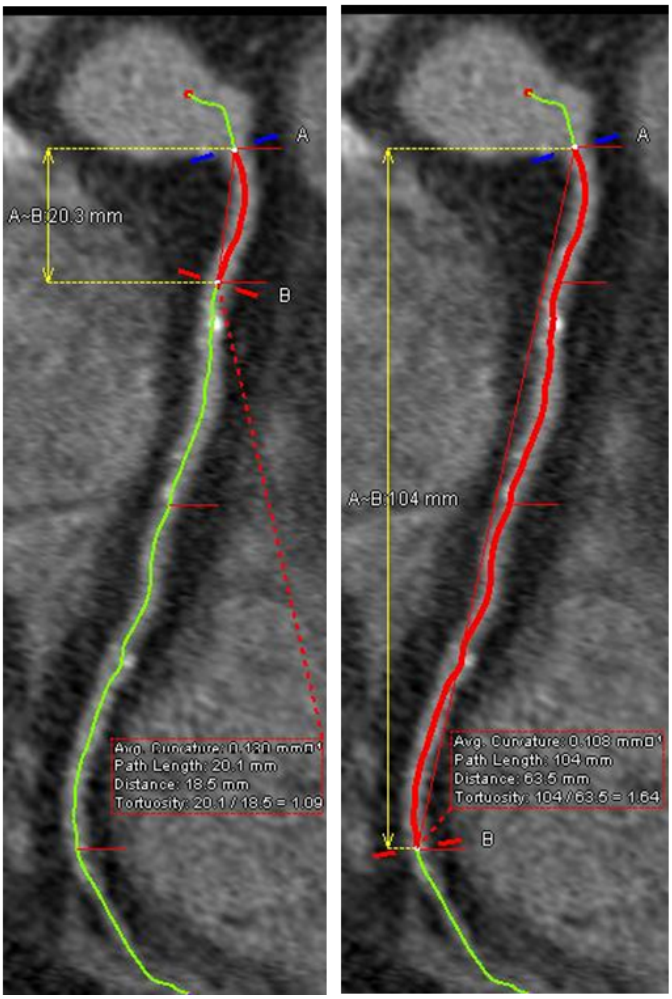

Figure 2.2: Example of the RCA in curved planar reformation (CPR). Segments are separated by red markers. Curvature and tortuosity are measured for segment (left image) and whole vessel (right image). The measured segment from this image has a length of 20.1 mm, curvature of 0.130 mm^{-1}, and tortuosity of 1.09. The whole vessel has a length of 104 mm, curvature of 0.108 mm^{-1}, and tortuosity of 1.64.

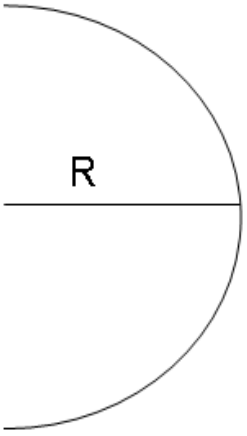

(a) Curvature (κ), defined as inverse radius of curvature (R).

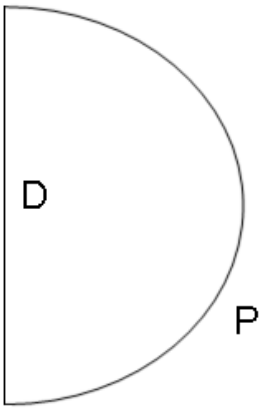

(b) Tortuosity (T), defined as path length (P) divided by straight distance (D).

Figure 2.3 Basic definitions of curvature and tortuosity. More detail is provided in Chapter 3.

	All patients (n=73)
Age (years)	64.8 ± 8.1
Gender (male)	56 (76.7%)
Body mass index (kg/m2)	26.2 ± 3.8
Systolic blood pressure (mmHg)	140 ± 24
Diastolic blood pressure (mmHg)	79 ± 9
Hypertension	60 (82.2%)
Cholesterol (mmol/L)	4.7 ± 1.2
Triglyceride (mmol/L)	1.50 [.94 ; 2.25]
HDL cholesterol (mmol/L)	1.2 ± .4
LDL cholesterol (mmol/L)	2.9 ± .9
Dyslipidemia	68 (93.2%)
Glucose (mmol/L)	5.6 [5.1 ; 6.2]
Diabetes mellitus	7 (9.6%)
Smoking	24 (32.9%)

Table 2.1: Clinical characteristics of the study population. Continous variables are expressed as mean ± standard deviation or median [25^{th} ; 75^{th} percentile], dichotomous variables are expressed as percentages. HDL: high density lipoprotein; LDL: low density lipoprotein.

To investigate an association between significant stenosis and curvature/tortuosity, a linear mixed model was applied on curvature and tortuosity separately. The analysis was performed on results at the level of segments and at the level of arteries (RCA, LM, LAD, and LCx). The curvature and tortuosity measurements may be correlated since repeated measurements were obtained from each patient. To accommodate the correlations, a compound symmetry correlation was selected at the segment level and a heterogeneous compound symmetry correlation at artery level. The results on curvature were logarithmically transformed, and a double logarithmic transformation was used for tortuosity, to better resemble normal distribution. The effect of significant stenosis was implemented in the model as a fixed effect and as an interaction with segments or with arteries. Association and interaction analyses were corrected for age, sex and hypertension. All statistical tests were two-sided with p<.05 as significance.

2.3 RESULTS

2.3.1 *Characteristics*

Seventy-three participants (76.3% males, mean age 64.8 ± 8.1 years) with scans reconstructed in end-diastolic phase were included in this sub-study. Patient characteristics are shown in Table 2.1. The prevalence of cardiovascular risk factors was high (Table 2.1). In total 730 segments were assessed of which 81 (11.1%) were excluded due to small diameter (<1.5 mm) and 50 (6.8%) because of the inability to perform proper centerline segmentation due to acquisition related artifacts. Overall, the median curvature and tortuosity with [25^{th} ; 75^{th} percentile] were .094

mm^{-1} [.071 ; .120] and 1.08 [1.04 ; 1.12] on segment level, and .096 mm^{-1} [.078 ; .118] and 1.18 [1.09 ; 1.42] on artery level (Table 2.2).

2.3.2 *Reproducibility and Reader Agreement*

The ICC results are provided in Table 2.3. The overall ICC showed high intra-reader agreement (ICC>.8) for tortuosity and measurements. Inter-reader agreement is strong for curvature (ICC=.73) and almost perfect for tortuosity (ICC=.92). Bland-Altman analysis showed mean inter-reader difference for curvature and tortuosity of respectively .004 (95% CI: -.05, .06) and .02 (95% CI: -.16, .21). Mean intra-reader difference for curvature and tortuosity were respectively -.001 (95% CI: -.04, .04) and .001 (95% CI: -.18, .17). Bland-Altman plots are given in Figure A.3-A.6.

2.3.3 *Association between Significant Stenosis and Coronary Geometry*

We observed a significant association between significant stenosis and curvature both at segment level (p<.001) and artery level (p=.002) (Table 2.4). In addition there was an association between significant stenosis and tortuosity when analyzed at the segment level (p=.016). Patients with a significant stenosis had 16.7% more curvature at segment level than patients without stenosis. The effect of tortuosity on stenosis is modified by the segment (interaction p=.041). Investigating segments demonstrates that the LM (segment 5) and mid-LAD (segment 7) are more affected by a significant stenosis in the presence of tortuosity, while other segments are not. The significant interaction (p=.035) for tortuosity at artery level for normal stenosis indicates that the effect is not the same across arteries. However, the overall effect of stenosis on the geometrical parameters is not significant.

2.3.4 *Association between Presence of Plaque and Coronary Geometry*

An association between plaque and curvature at both segment (p<.001) and artery level (p<.001) was demonstrated (Table 2.5). Association between plaque and tortuosity was only found at

Table 2.2: Nonparametric descriptive statistics of included segments and arteries in this study.

Vessel	**Number of inclusions**	**Curvature median** [25^{th}, 75^{th} percentiles]	**Tortuosity median** [25^{th}, 75^{th} percentiles]
RCA	57	.093 [.071, .101]	1.80 [1.61, 2.10]
LM	70	.137 [.110, .182]	1.07 [1.04, 1.12]
LAD	70	.086 [.074, .104]	1.15 [1.12, 1.21]
LCx	53	.086 [.070, .103]	1.21 [1.14, 1.28]
Overall Segment	599	.094 [.071, .120]	1.08 [1.04, 1.12]
Overall Artery	250	.096 [.078, .118]	1.18 [1.09, 1.42]

Table 2.3: Intra- (IA) and inter-reader (IE) variability for curvature (κ) and tortuosity (T) measurements determined by intraclass correlation coefficient (ICC).

		Seg 1	Seg 2	Seg 3	RCA	LM	Seg 6	Seg 7	Seg 8	LAD	Seg 11	Seg 13	LCx	Overall
IA	κ	.848	.841	.807	.921	.739	.832	.837	.907	.928	.866	.829	.846	.869
	T	.797	.499	.630	.751	.693	.864	.851	.917	.861	.887	.709	.778	.929
IE	κ	.736	.851	.762	.919	.389	.663	.580	.914	.879	.419	.540	.535	.731
	T	.910	.554	.551	.897	.232	.847	.649	.685	.615	.908	.396	.619	.919

Table 2.4: Association of stenosis with curvature and tortuosity corrected for age, sex, and hypertension. The 25^{th} and 75^{th} percentiles are shown between brackets. Significance is indicated with an asterisk.

Outcome	Stenosis	Analysis on segment level			Analysis on artery level		
		Estimate	Association (p-value)	Interaction (p-value)	Estimate	Association (p-value)	Interaction (p-value)
Curvature	>50%	1.067 [.992, 1.147]	.080	.943	1.042 [.968, 1.121]	.273	.183
	>70%	1.167 [1.088, 1.251]	<.001*	.421	1.138 [1.049, 1.235]	.002*	.106
Tortuosity	>50%	1.092 [.932, 1.282]	.274	.395	1.113 [.985, 1.257]	.086	.035*
	>70%	1.279 [1.097, 1.491]	.016*	.041*	1.105 [.964, 1.267]	.149	.056

Table 2.5: Association of plaque presence with curvature and tortuosity corrected for age, sex, and hypertension. The 25^{th} and 75^{th} percentiles are shown between brackets. Significance is indicated with an asterisk.

Outcome	Analysis on segment level			Analysis on artery level		
	Estimate	Association *(p-value)*	Interaction *(p-value)*	Estimate	Association *(p-value)*	Interaction *(p-value)*
Curvature	1.176 [1.106, 1.251]	<.001*	.066	1.161 [1.078, 1.250]	<.001*	.136
Tortuosity	1.308 [1.142, 1.498]	<.001*	.013*	1.096 [.969, 1.241]	.145	.237

segment level (p<.001). The group with a plaque has a 17.6% higher curvature at segment level then the group without plaque. The p-value of .013 for the interaction of plaque and segments for tortuosity indicates that the effect of plaque is not the same across segments. Investigating the segments demonstrates that the proximal RCA (segment 1), LM (segment 5) and mid LAD (segment 7) are significantly affected by plaque, while the other segments are not significantly affected by plaque. The average effect of plaque on tortuosity on segments is an estimated 30.8% increase.

2.4 DISCUSSION

In this study, we used non-invasive coronary CT angiography (cCTA) measurements to assess the association of coronary artery geometry with significant stenosis and plaque presence. Our

results suggest that there is an association between significant stenosis and curvature both at segment and artery level. Furthermore, presence of plaque is associated with both curvature (for segments and arteries) and tortuosity (only segments).

Traditionally coronary artery plaque development and distribution of atherosclerotic lesions have been considered to be influenced by hemodynamics.[17] Several studies investigated the relationship between WSS and the presence and location of atherosclerosis in the coronary arteries, and demonstrated an inverse relationship of WSS with atherosclerosis.[6, 21, 23, 30–33] This endorses the idea that CAD is more advanced where WSS is low. However, not all studies support the theory that low WSS and vessel wall morphology are at least related, as reviewed by Peiffer *et al*.[17] For example, Gijsen *et al*. could not find any relationships with WSS and the wall thickness.[22] A small number of follow-up studies investigate the relationship between WSS and atherosclerosis. The most extensive follow up study observed plaque thickness change through 6 to 10 month periods.[34] They found that change in plaque area was not related with WSS. However, they related low WSS with decreased lumen area and high WSS with increased lumen area.

Although we investigated coronary geometry and its relation with CAD based on cCTA, the reference standard for coronary artery assessment has traditionally been ICA. This conventional technique provides two-dimensional images of the complex three-dimensional structure of the coronary artery tree, and is an invasive procedure that may cause complications in up to 2% of patients.[35] ICA is restricted to symptomatic patients suspected of significant CAD, thus rather late in the atherosclerotic process. Also, no information about the presence of plaques in the vessel wall is obtained in ICA.[36] An additional complicating factor is that scarce ICA studies in this field report different methods to evaluate coronary curvature and tortuosity, ranging from visual analysis of the numbers of bends to measurement of a radius of curvature on two-dimensional images. Studies on shear wall stress are frequently using intravascular ultrasound (IVUS) to determine the three-dimensional geometry of the coronary artery lumen and wall. However, this technique is also invasive and requires pull-back of a catheter with an ultrasound probe to image the arteries. Acquired ultrasound slices of the artery are subsequently projected into 3D space based on the ICA measurement and the position of the IVUS catheter obtained from pull-back steps. Although visualization of a 3D vessel wall representation is possible with high quality, calcifications hamper the visualization of the vessel wall, location of the slices in three-dimensional space are computed and not exactly known, and this technique is invasive.[6] Coronary CT angiography is a non-invasive imaging technique that is faster, cheaper, and causes less complications than ICA or IVUS. Recent technical developments have made cCTA an acceptable alternative for coronary artery assessment.[37] cCTA is also applicable in lower-risk patients than those undergoing ICA, especially for exclusion of CAD. Thus, a wider range of atherosclerotic disease, from mere presence of plaque to stenosis, can be assessed and correlated with coronary artery geometry.

In our study we calculated the curvature and tortuosity based on a vessel centerline extracted from the cCTA data. There are various methods to calculate the tortuosity and curvature, all based on a spatial representation of the vessel (i.e. vessel centerline or vessel medial line). Tortuosity (Figure 2.3b) was defined as the ratio of path length (P) divided by the straight line distance (D) in some studies as it is in our study.[38–40] Similar ratios are also used, like the tortuosity index of $100 \times (P - D)/D$ by Malvè *et al.*[5] However, some studies define tortuosity as the bend angle and/or the number of bends.[16, 24, 41–43] Wolf *et al.* defined tortuosity as the inverse of the radius of curvature,[41] which is more frequently and also by us referred to as curvature. The exact calculation of curvature is more complex since the radius of curvature is a variable parameter for each point of a vessel, and elaborated more upon in section 3.2.3. To maintain the common definition of curvature as departure from straightness, curvature can be calculated using polynomial curve fitting applied to the extracted centerline, or an average between individual points of the centerline with different scale setting. In the first case, local curvature is computed by the formulations containing derivatives of the centerline curve at the desired location.[6, 38, 44–48] Our method involves the second case with an average (Menger's) curvature with a 5 mm scale between points.[27] Although different scale settings can yield different results, this setting should be robust enough not to affect our results significantly or limit the accuracy of our method.

Striking points in this study are that *(1)* analysis on segment level reveals a stronger relationship between vessel geometry and significant stenosis than on artery level, and *(2)* curvature is stronger associated with significant stenosis than tortuosity. The same relationship and association is observed when gender, age, hypertension and smoking habit are taken into account. These results imply that local geometry of segments instead of whole artery geometry is related with plaque development. An explanation why curvature is more strongly related, might be that curvature computation is more sensitive than the tortuosity measurements. Tortuosity is simply the ratio of path to the length. It can not differ too much with small curves on the vessel. On the other hand, the curvature calculations were very sensitive to any curvature on the vessel and the final curvature on a path is the average of all the curvature measurements on the segment or the artery.

A shortcoming of this study is that, although the patients were asymptomatic for coronary artery disease, they did have symptomatic peripheral artery disease. This could provide a bias in the measurements and not present a true, asymptomatic, control group for the non-calcified segments.

In this study, we only used static information of the coronary artery anatomy without hemodynamic information to assess the WSS. Although the hemodynamic reasoning behind plaque development is used as a rationale for this study, we bypassed certain methodologies and tried to find predictors of or potential risk factors associated with CAD. Also, there are no follow-up scans available in order to assess plaque development, making it difficult to predict whether curved/tortuous vessels have a tendency to develop significant stenosis or if it may be

the other way around. Based on a study design as used here, only associations between (the extent of) CAD and the geometry of the coronary arteries can be given.

The software used in this study enables evaluation of vessel geometry in relation with presence of stenosis and atherosclerotic plaque more easily than invasive techniques. A follow-up study should contribute to the question whether increased curvature is a prediction of plaque development or its result. Information of dynamic coronary geometry can also be quantified with the current technique, and should provide additional insights in the relationship between CAD and geometrical changes during the cardiac cycle.

CHAPTER 3

Geometrical Differences in the Cardiac Cycle

Manuscript title: Geometrical differences of the coronary arteries in the cardiac cycle

Authors: JK van Zandwijk[1,2], V Tuncay[1], CH Slump[2], M Oudkerk[1], R Vliegenthart[1,3], PMA van Ooijen[1,3]

– To be submitted to *Annals of Biomedical Engineering* –

3.1 INTRODUCTION

CAD is the most common type of heart disease and leading cause of death worldwide.[4] The development of coronary artery plaque has been proposed to be related to hemodynamics and geometry of the coronary arteries, but these relationships are complex and still subject of debate.[6]

Previous hemodynamic studies using flow simulations in static vessel models have suggested an association between low WSS and plaque development in coronary arteries. Thus, there may be preferred sites for plaque development.[5, 6, 16, 20, 47] In studies on coronary hemodynamics in simulations incorporating cardiac motion, the importance of considering physiologically realistic flow and vessel motion has been stressed. This implies the need for *in vivo*, patient studies.[14, 19, 46, 49, 50]

ICA is still considered the golden standard for the diagnosis CAD, but is limited by its invasiveness and lack of information about plaque characteristics.[36] Scarce data are available from ICA studies about coronary geometry and the relation with CAD-related events. Zhu *et al.* catalogued human coronary artery geometry,[45] and O'Loughlin *et al.* found that segment length can be used to predict the location of future culprit lesions causing myocardial infarctions.[51] cCTA is a non-invasive imaging technique that is faster and with less discomfort to the patient, and is nowadays an accepted alternative in coronary artery assessment.[37] Three-dimensional change in coronary artery geometry during the cardiac cycle can be investigated using cCTA with retrospective ECG gating, however at the expense of increased radiation dose. O'Loughlin *et al.* correlated the ratio of coronary artery length between end systole (ES) and end diastole (ED) with location of lesions on dual-source CT.[52] In this study, only information

[1] Center for Medical Imaging - North East Netherlands (CMI-NEN), University Medical Center Groningen
[2] Technical Medicine Faculty, University of Twente
[3] Department of Radiology, University of Groningen, University Medical Center Groningen

about the length of coronary segments was obtained, rather than specific geometric information. Dedicated software packages now enable the extraction of quantifiable three-dimensional parameters of vessel geometry, which can be derived from multiple phases of the cardiac cycle when retrospectively ECG-gated cCTA imaging is performed.

The current study focuses on the assessment of coronary artery geometry throughout the cardiac cycle based on cCTA. Our hypothesis is that there are quantifiable parameters describing coronary geometry that correspondingly account for varying geometry during cardiac motion. If the method presented here is robust, this can facilitate future detailed investigation of coronary hemodynamics and the relationship with the development of CAD *in vivo*.

3.2 METHODS

3.2.1 *Patients*

Participants involved in different scientific studies from April 2006 until April 2007 were included in this retrospective study.[53–55] Approval from the Medical Ethical committee was available for each study. Informed consent was obtained from all patients as part of these studies. Patients were either planned for elective conventional ICA,[53] had a high probability of CAD,[54] or were assessed at the emergency department because of acute chest pain.[55] cCTA was performed at a single center. Patients were excluded if they had previous heart surgery or previous percutaneous coronary intervention (PCI), or if they had a coronary anomaly on cCTA.

3.2.2 *Computed Tomography*

cCTA was performed on a first-generation dual-source CT scanner (SOMATOM Definition, Siemens, Erlangen, Germany) using a standardized protocol. This protocol involved retrospective ECG gating with an ECG pulsing window set at 20-70%. Patients were administered beta-blockers (metoprolol, 5-20 mg) intravenously if the heart rate was above 65 beats per minute. Table pitch was dependent on the heart rate, with a cranio-caudal scan direction starting above the coronary ostia and ending below all cardiac structures at the diaphragm. All patients were given sublingual nitroglycerin (0.4 mg) prior to the scan protocol. To be included in this study, reconstructions should at least have been made at every 10% of the RR-interval, with a slice thickness of 2.0 mm with 64 x 0.6 mm collimation. Contrast enhanced scans were made with a non-ionic contrast agent (Iomeprol 400 mg I/ml, Iomeron® 400, Bracco, Italy) with contrast volume and infusion rate individually calculated for each patient. Piers *et al*.[53] described the scan protocol in more detail. In clinical setting, the cCTA examination was assessed for presence and severity of CAD by an attending radiologist with at least two years experience in cardiac CT.

3.2.3 *Geometrical Parameters*

Reconstructed cCTA data were loaded onto a dedicated workstation (Aquarius iNtuition, TeraRecon, Ver.4.4.11, San Mateo, USA). Post-processing included auto-removal of the ribcage and extra-cardial structures. Automatic built-in threshold-based left ventricular ejection fraction (LVEF) analysis function automatically determined the ES and ED phases of the cardiac cycle based on respectively the minimum and maximum filling of the left ventricle. For the current study, when the reconstruction quality of the coronary arteries in the automatically determined ES or ED phase was too low, another phase with diagnostic depiction of the coronary arteries was selected up to two phases shifted from the minimum or maximum filling. This was assessed for each coronary artery individually. If optimal quality could not be obtained based on these restrictions, the coronary artery was excluded from further analysis.

The resulting ES and ED phases were used for detailed inspection of the coronary arteries and its individual segments, according to the 15-segment modified AHA-classification.[1] Only the largest segments that exhibit the least variation in presence and dominance were assessed. For the RCA these are the proximal, mid-, and distal segment. For the left coronary artery these are the LM artery, proximal, mid-, and distal segments of the LAD artery, and the proximal and distal segments of the LCx artery. On artery level, the RCA, LAD, and LCx were assessed separately. Due to the wide variety in coronary artery branching configurations between individuals, we terminated segments at other side branches of one individual in both phases maintain comparable segments with adequate length. In cases where no side branches where present to terminate the segment, we maintained equal pre-set lengths in both ES and ED phase to make sure comparable parts of the vessel were considered (mainly the proximal RCA, distal LAD, and distal LCx). Segments were terminated or excluded if they were smaller than 1.5 mm in average diameter, had a bad reconstruction quality due to the presence of artefacts or incorrect centerline extraction, or were not visible at all. Arteries were excluded if one or more segments could not be assessed.

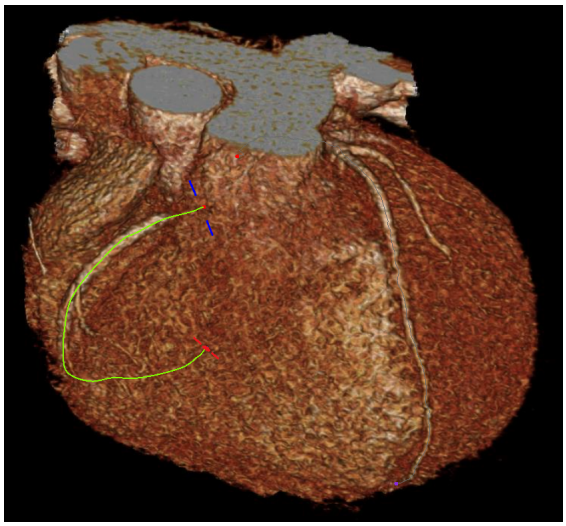

Figure 3.1 Example of a volume rendered 3D image with centerline extractions of the RCA (selected) and LAD at 70% of the RR-interval (ED).

The coronary arteries were selected on the 3D volume rendered reconstruction (Figure 3.1) or transverse slices in the relevant phase in order to initiate automatic centerline extraction of an artery. The CPR view was reconstructed based on this centerline, after which it was manually

adapted to ensure the most appropriate implementation of this centerline. Markers were applied at each beginning and endpoint of a segment, based on branching of the artery from the aorta, and side branches. If no side branches existed at the final segment of an artery, a diameter of less than 1.5 mm was used as endpoint in both phases. Measurements were performed for each segment and each entire artery, apart from the LM artery.

Basic definitions of this geometrical parameters have been given in Chapter 2, where more detail of these parameters is provided in this section. The centerline can be described as a parametrically defined space curve in three dimensions in Cartesian coordinates given by $\gamma(t) = (x(t), y(t), z(t))$, with t ranging from 1 to n points of the centerline. The following geometric parameters were assessed: path length (P in mm), mean curvature (κ in mm^{-1}, see Equation 3.1), tortuosity (T, see Equation 3.2), and number of inflection points of the centerline with the straight connection between begin- and endpoint on CPR view (see Figure 3.2 for an example).

$$\kappa = \sum_{i=1}^{n} \frac{4A}{|\gamma(t_i - s) - \gamma(t_i)||\gamma(t_i) - \gamma(t_i + s)||\gamma(t_i + s) - \gamma(t_i - s)|} \tag{3.1}$$

$$T = \frac{\sum_{i=1}^{n-1} \sqrt{(x(t_i) - x(t_{i+1}))^2 + (y(t_i) - y(t_{i+1}))^2 + (z(t_i) - z(t_{i+1}))^2}}{\sqrt{(x(t_1) - x(t_n))^2 + (y(t_1) - y(t_n))^2 + (z(t_1) - z(t_n))^2}} \tag{3.2}$$

Equation 3.1 denotes Menger's curvature [27] with a 5 mm scale applied as s and with A the area of the triangle spanned by the three corresponding points $\gamma(t_i - s)$, $\gamma(t_i)$ and $\gamma(t_i + s)$. The numerator in Equation 3.2 denotes the length of the centerline (P), whereas the denominator denotes the great circle chord length (i.e. straight distance, D) between the beginning and endpoint of a segment or artery. The number of inflection points is determined by the maximum number of intersections (inflection points) that the straight connection between beginning and endpoint has with the centerline when rotating the CPR view (Figure 3.2).

3.2.4 *Statistical Analysis*

Normality of the data was assessed with the Shapiro-Wilk analysis. With current arteries and segments sample size, data are considered to have a normal distribution when the test statistic is greater than 0.9. Curvature, tortuosity and number of inflection points were assessed in ES and ED, and differences were calculated as the value in ES minus the value in ED. Normally distributed data of the differences between ES and ED were tested with the paired sample T-test, whereas skewed data were tested with the non-parametric Wilcoxon signed-rank test.

All statistical analyses were performed in IBM SPSS Statistics version 22.0.0.1 (SPSS Inc, Chicago, USA). Significance for difference was expressed with p-values, where a two-tailed p-value of <.05 was considered significant.

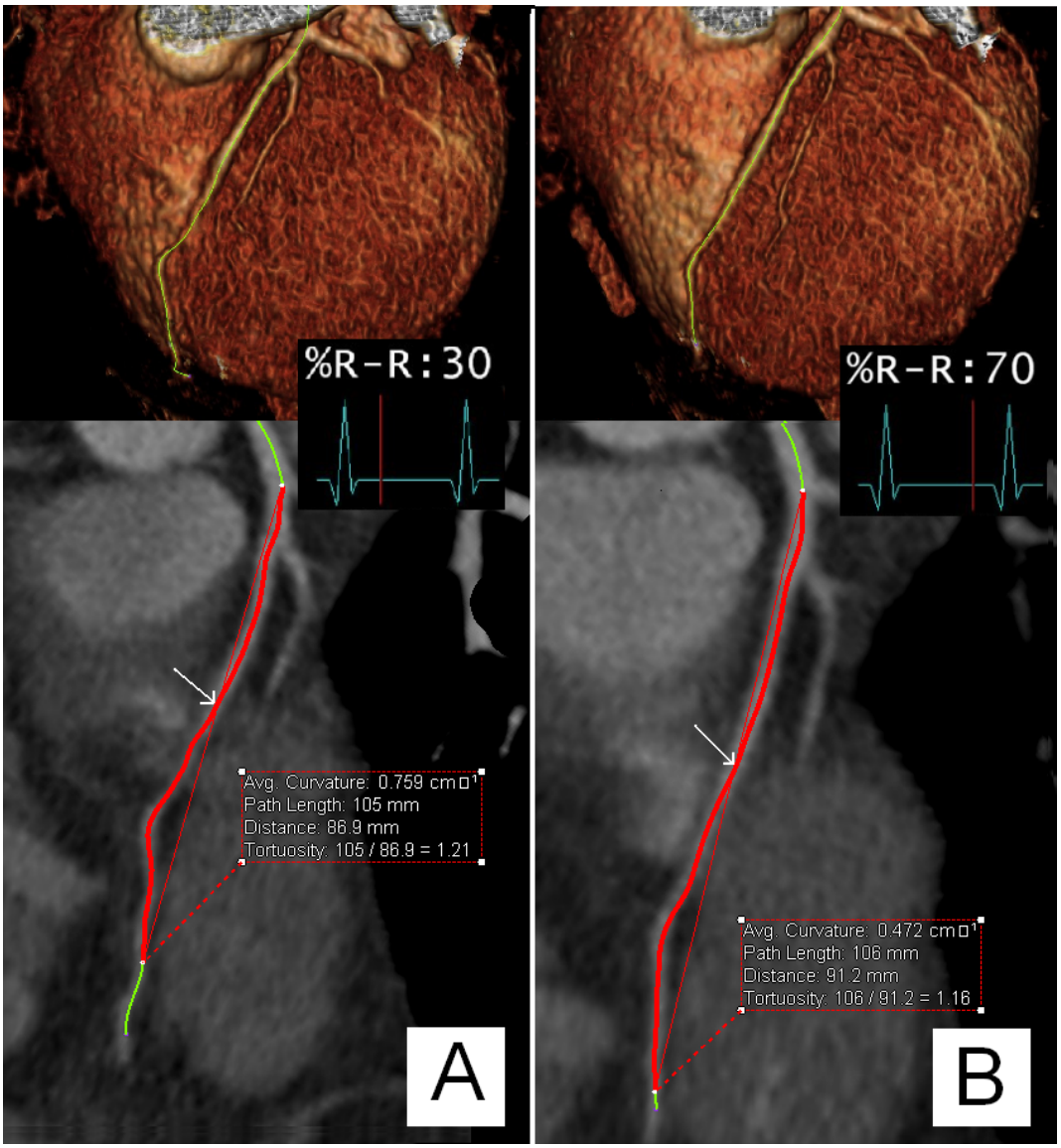

Figure 3.2 Geometry measurements of the LAD **(A)** at 30% in ES and **(B)** at 70% in ED. According to these measurements, the LAD has 1% less path length, 26% higher curvature, and 3% higher tortuosity in ES. The white arrows indicate one inflection point in both phases.

3.3 RESULTS

Seventy-one patients in whom at least one artery could be assessed were included in this study. Mean age was 62.2 ± 9.9 years and 87.3% were males. In total 213 arteries and 639 segments were assessed of which 137 arteries (64.3%) and 456 segments (71.4%) could be included. The group of arteries consisted of 53 RCA (38.7%), 45 LAD (32.8%), and 39 LCx arteries (28.5%). In ES, the segments were most frequently best assessable at 40% of the RR interval (n=227, 49.8%, range 5-60%). In 11.6% of the segments a deviation was needed from the original, software-indicated ES phase due to low reconstruction quality or motion artefacts. In ED, the segments were most frequently best assessable at 90% of the RR interval (n=172, 37.7%, range 70-110%). In 66.9% of

Table 3.1: Outcomes of the measured parameters in ES and ED phases on artery and segment level, depicted as mean ± standard deviation. P, path length (mm); κ, curvature (mm^{-1}); T, tortuosity. Significant difference is indicated with an asterisk.

		Arteries (n=137)		Segments (n=456)	
Parameter	**Phase**	**Outcome**	**p-value**	**Outcome**	**p-value**
P	ES	95.8±26.8	0.699	32.4±17.9	0.617
	ED	95.9±26.9		32.5±17.7	
κ	ES	0.079±0.022	<0.0001*	0.085±0.033	<0.0001*
	ED	0.071±0.018		0.078±0.031	
T	ES	1.46±0.37	<0.0001*	1.12±0.11	<0.0001*
	ED	1.42±0.37		1.10±0.10	

Table 3.2: Outcomes of the measured parameters in ES and ED phases for each individual artery, depicted as mean ±standard deviation. P, path length (mm); κ, curvature (mm^{-1}); T, tortuosity. Significant difference is indicated with an asterisk.

		RCA (n=53)		LAD (n=45)		LCx (n=39)	
Parameter	**Phase**	**Outcome**	**p-value**	**Outcome**	**p-value**	**Outcome**	**p-value**
P	ES	112.3±18.9	0.490	99.1±22.5	0.238	69.7±20.3	0.704
	ED	112.0±19.0		99.6±22.3		69.8±20.9	
κ	ES	0.077±0.018	0.021*	0.088±0.025	<0.0001*	0.071±0.019	0.032*
	ED	0.073±0.016		0.073±0.021		0.067±0.018	
T	ES	1.86±0.28	0.0002*	1.22±0.07	<0.0001*	1.19±0.13	0.001*
	ED	1.81±0.30		1.17±0.06		1.17±0.12	

the cases there was a deviation from the original ED phase. Although the assessed cases at 110% (i.e. 10%) of the RR-interval (n=41, 9.0%) are strictly part of the subsequent cardiac cycle, they were found to have a sufficient filling of the left ventricle to be assessed in this phase.

Table 3.1 and Table 3.2 show overall values for path length, curvature, and tortuosity in ES and ED on (individual) artery and segment level. Figure 3.2 depicts a patient example of geometrical parameters in ES and ED.

3.3.1 *Path Length*

Path length differences between ES and ED were normally distributed for arteries and segments. Path length for ES and ED were similar on artery level (p=0.64), including the three individual arteries, and on segment level (p=0.62).

3.3.2 *Curvature*

Curvature in ES and ED and differences in curvature were normally distributed. Compared to the ED phase, mean curvature was 10.5% higher in the ES on artery level (p<0.0001), and 8.9% on segment level (p<0.0001) (Table 3.1). The most pronounced difference between ES and ED was

found for the LAD (20.8%), while differences were lower for the RCA (4.8%) and the LCx (6.0%) (Table 3.2).

3.3.3 *Tortuosity*

Tortuosity differences were normally distributed. The mean tortuosity was 2.8% higher in ES than in ED on artery level ($p<0.0001$), and 1.6% on segment level ($p<0.0001$) (Table 3.1). For individual arteries, mean tortuosity was 1.5-4.2% higher in the ES than in ED (Table 3.2).

3.3.4 *Inflection Points*

The difference in number of inflection points was not normally distributed on artery and on segment level (Shapiro-Wilk statistic value 0.755 and 0.564, respectively both $p<0.001$). The number of inflection points per artery ranged from 1 to 5 (median, 2) for both ES and ED (Figure 3.3). On segment basis, 0 to 6 inflection points were found in ES, and 0 to 5 in ED (median, 0) (Figure 3.4). The median number of inflection points was higher in ES than in ED on artery and on segment level (both $p<0.001$). Increase in number of inflection points in ES phase was found for the RCA ($p<0.05$) and the LAD ($p<0.001$), but not for the LCx ($p=0.405$).

On segment level, the difference in inflection points was not normally distributed with a Shapiro-Wilk statistic value of 0.564 ($p<0.001$). The range of number of inflection points was from 0 to 6 in ES, and 0 to 5 in ED, with in both phases a median value of 0. Figure 3.5 depicts for each segment the paired number of inflection points in both phases. Non-parametric Wilcoxon signed-rank test showed that in ES there were significantly more inflection points than in ED ($p<0.0001$).

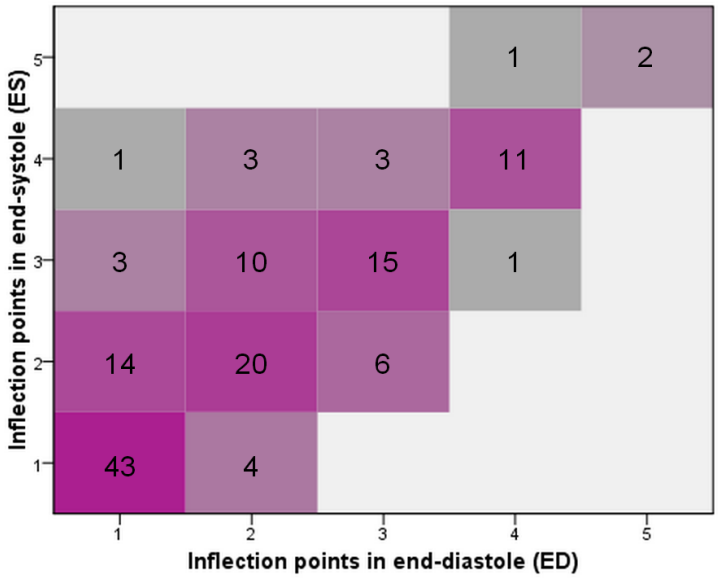

Figure 3.3: Map of the number of inflection points in ES and ED for all arteries together. The numbers in the boxes depict the amount of times that specific combination was observed. Darkness in the boxes is linked with natural logarithmic transformed numbers in the relevant box.

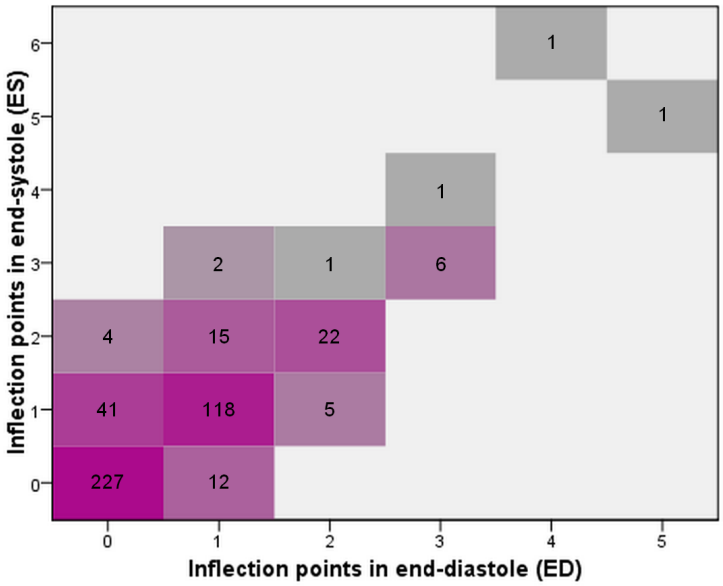

Figure 3.4: Map of the number of inflection points in ES and ED for all segments. The numbers in de boxes depict the amount of times that specific combination was observed. Darkness in the boxes is linked with log transformed numbers in the relevant box.

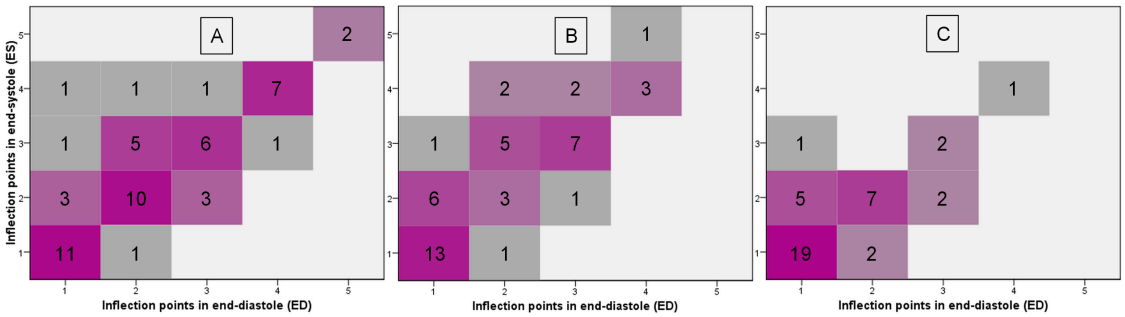

Figure 3.5 Map of the number of inflection points in ES and ED for **(A)** the RCA, **(B)** the LAD, and **(C)** the LCx. The numbers in the boxes depict the amount of times that specific combination was observed. Darkness in the boxes is linked with logarithmic transformed numbers in the relevant box.

3.4 DISCUSSION

This study shows that the geometry of the coronary arteries is quantifiable using four-dimensional dual-source CT datasets and confirms our hypothesis that the coronary arteries have an alternating geometry during the cardiac cycle. By measuring parameters describing the geometry, the possibility arises to correlate these findings with the presence and preferred sites of plaque development in the coronary arteries.

The novelty of this research resides in its uniqueness to quantify characteristics of the coronary arteries describing their movement during the cardiac cycle in a non-invasive way and in three dimensions, and derive new quantitative imaging biomarkers based on regular coronary CT scans. To our knowledge this is the first patient study quantifying coronary geometry through the cardiac cycle based on straightforward post-processing of non-invasive imaging data. Previous studies that focused on the relation between vessel geometry, corresponding hemodynamics,[14, 46, 50, 53] and the relation with plaque development [5, 6, 15] were often

based on computational fluid dynamics, and were thus accompanied by modeling assumptions requiring a considerable amount of time and computational capacity.[5, 56] These studies found that hemodynamic and geometrical parameters can be linked with (early) plaque development, but conclusions were drawn based on modeling or static approaches of the coronary arteries. A striking advantage of this study is the use of dedicated, commercially available software on cCTA datasets, which makes this method immediately clinically applicable. The association of dynamic vessel geometry with plaque development can thus be investigated, and more evidence can be obtained about the process of atherosclerosis that may lead to identification of potential high-risk sites or patients.

Based on ECG-gated CT datasets, 40% and 90% of the RR interval were the most frequently identified phases for evaluation of the coronary arteries in end-systole and end-diastole, respectively. Although this may seem late in the cardiac cycle, these percentages correspond with the results of Juergens *et al.*,[57] who found ES and ED phases ranging from respectively 20-35% and 75-90% of the RR interval. Furthermore, some selections of ED phase turned out to be at 110% of the RR interval. This may possibly imply incorrect registration of the ECG with the reconstructions. Since we maintained consistently the phase with minimal and maximal filling of the left ventricle with less possible variation in phase, our results are robust enough to represent the actual ES and ED phases, as we expect regression to the mean and lessening of the associations if the selected phases were actually not ES and ED.

Geometry changed in terms of curvature and tortuosity on both artery and segment level, but there were no significant differences for all arteries. However, it could be interesting to observe these geometric parameters for each individual segment. We combined the measurement of all these segments to increase our sample size, since some segments were frequently hard to assess. Besides, the left main artery (segment 5) and proximal LAD (segment 6) are often shorter than 20 mm, making them more sensitive for curvature and tortuosity measurements, increasing the risk of upward peaks in case of incorrect parts of the centerlines. With sufficiently large sample sizes it could be interesting to investigate whether segments more closely adjacent to the myocardium experience larger geometric differences than segments closer to the coronary ostia. For example, Zhu *et al.* measured geometry of the proximal, mid, and distal segments separately of the RCA and LAD in one phase and found for instance a two-fold difference in maximum curvature in LAD segments between individuals.[45] They state that a particular geometrical feature must exhibit large variability between vascular regions or indivuals, if it should be considered as an atherosclerotic risk factor. They also suggested to add a dynamic dimension in addition to their work, which can create even more variability. In their study, biplane cineangiography was used for the quantifications, which is invasive in contrast to CT and so only applicable in selected patients at high suspicion of CAD. Furthermore, this involves two projection directions, requiring additional reconstruction algorithms to obtain three-dimensional information.[47]

A particular strength of this study resides in the fact that coronary arteries were geometrically quantified in four dimensions based on cCTA data involving multiple phases of the cardiac

cycle. The only patient study somewhat comparable to ours was conducted by O'Loughlin *et al.*,[52] but they only investigated the length of segments, and only included a few segments of the coronary tree. They found that the ratio of length in end-systole divided by the length in end-diastole was correlated with the location of CAD, but only for the first two segments of the LAD and LCx. Our method involves more detailed and three-dimensional geometric information in terms of curvature, tortuosity, and inflection of both segments and (multiple) arteries. Based on the anatomical properties significant differences in vessel and segment lengths between ES and ED are not expected. Our vessel length measurements support this assumption. Therefore, the method used to perform the segmentation of arteries and segments can be classified as a valid and robust method. As a results, geometric information of segments and arteries can be used to investigate possible associations with stenosis sites.

Like more arterial geometry studies, we performed measurements based on a semi-automatically extracted centerline from the CT datasets. The centerline creation did not always yield an accurate result. Especially extraction of severely diseased coronary arteries was frequently incorrect, thus requiring manual adaptation of the centerline to achieve a better match with the vessel trajectory. This could have affected our geometric measurements. Corresponding segments from the same patient were equivalently adapted in both phases to minimize intra- and inter-observer variability, but this is still a possible shortcoming of the study since variability was introduced. Because of our method selecting segments where we take in consideration different anatomical configuration between individuals, length measurements are less likely to differ between phases, in contrast to the previous mentioned study of O'Loughlin *et al.*[52] They included only the segments with highest chances of a visualized bifurcation (i.e. first two segments of the LAD and LCx), to acquire more reliable results when it comes to coronary segment length. Since plaques may develop throughout the coronary artery system, we decided to investigate as many segments larger than 1.5 mm as possible. Although not significant for all arteries or segments, path length was smaller in ES, suggesting slight compaction of the endothelial cells in the vessel wall.[58] This also corresponds with previous studies that related compression of coronary segments with significant stenosis.[52, 59]

Our method of describing the coronary geometry was mainly based on the curvature and tortuosity parameters derived from a spatial representation of the vessel (i.e. vessel centerline or vessel medial line). Tortuosity in coronary arteries has previously been assessed based on the number of bends in the vessel.[16, 24, 43, 60] The measurements of Li *et al.* for example are therefore substantially differing from ours, resulting in a more tortuous LAD than RCA based on their tortuosity definition.[24] We implemented tortuosity as ratio of path length (P) divided by the straight distance (D), which has also been applied in larger blood vessels.[38–40] However, this ratio was initially implemented to study tortuous iliac arteries, which are compared to coronary arteries mainly oriented in the anatomic coronal plane. Due to the curved course of the coronary arteries, the straight distance directly traverses the heart, making this parameter less relevant. Ideally, we should have used the great circle distance with respect to the surface

of the heart over the great circle chord length to depict a normal course of an artery and to quantify its deviation from this path. Furthermore, curvature calculation was implemented as departure from straightness, using the extracted centerline as a polynomial fitted curve in multiple studies.[38, 44–46, 48, 61] Our method averages the Menger's curvature with 5 mm scale between points, which is an adequate and robust option in order to not significantly affect our results or limit the accuracy of our method.

We addressed the question whether coronary geometry would be quantifiable in both ES and ED. The ES phase showed higher values for both curvature and tortuosity compared to the ED phase, meaning that arteries and segments are more curved and tortuous in end-systole. Maximal expansion of the heart muscle in ED and thus straightening the coronary arteries is thought to be the main contributor of this observation. No significant differences were found in path length on segment and artery level, indicating that the straight distance between begin and endpoint is the changing factor in tortuosity. It is expected that when individual segments are considered, not all of them will still show these significant deviations between the two phases, depending on the proximity to the myocardium. Varying straight distance can be a quantitative of vessel compression and more sites of (temporary) wall shear stress. This can be an important mechanical stress inducing plaque development.

The inflection points that were measured are a more subjective quantification, indicating that certain segments and arteries (especially the LAD) are more compressed in ES than in ED. An equivalent parameter has only twice been introduced for femoral [62] and intracerebral vasculature,[63] but has never been applied for coronary arteries or linked with plaque development. However, compression of coronary arteries may be an indicator for more sites of low wall shear stress.[16] Therefore, this novel introduced parameter may help us in predicting future sites of CAD or potential obstructive vessels.

The choice of segments we made is arguable, since only the segments larger than 1.5 mm in diameter were measured. Side branches such as the posterior descending artery or first diagonal branch of the LAD can also have major clinical impact when they become stenosed since they can provide a large area of myocardium with oxygen. A geometric profile could also have been made of these and other branches, but these have been deliberately omitted from this study because of their large anatomic variation, requiring larger study samples. In future studies the differences in coronary geometry during the RR interval should be linked to the development and presence of CAD. The final aim would be to eventually draw a CAD risk profile for patients also including their coronary geometry. The clinical benefits our method provides are still to be demonstrated, in order to defend the use of additional radiation for evaluation of end-systole and end-diastole in cCTA.

CHAPTER 4

Coronary Plaques and the Relation with Dynamic Geometry

4.1 INTRODUCTION

The relevance of the CAD which forms the motive of this study has been referred to before in this thesis. What not has been addressed yet, is that almost all parts of the coronary arteries are a whole life-time in motion, which affects blood flow correspondingly. Therefore, movement of these arteries can result in stresses inducing coronary atherosclerosis.[59] There are multiple reasons for the uncertainties about involvement of (dynamic) coronary geometry in the development of CAD.[6] An examples is the lack of an adequate imaging modality and quantitative method that can map both characteristics of the vessel wall and stenosis degree, and provide information about three-dimensional geometric characteristics.

This study focuses more specifically on sites of plaque development in the coronary arteries. A method is established to quantify CAD and describe its relation with dynamic geometry. Our hypothesis is that the type, location, and severity of plaque development are related with dynamic geometry changes quantified on DSCT datasets. To investigate this relationship and uncover potential associations, CAD is quantified in an innovative way from a hemodynamic point of view. With this study also the association between static geometry and CAD is examined for robustness along with previous findings from Chapter 2, and whether dynamic geometry characteristics add relevant information to this association. The ultimate goal is to improve risk stratification of future CAD patients based on coronary geometry, which can affect the follow-up protocol for this group of patients.

4.2 METHODS

4.2.1 *Patients and Computed Tomography*

The same group of patients was used as described in Chapter 3, which were derived from several studies in the University Medical Center of Groningen [53–55]. That chapter also describes the used imaging protocol with relevant parameters, and assessment of dynamic coronary geometry

in the cardiac cycle. Parameters describing change in coronary geometry were used here to investigate associations with presence of (the most obstructive) plaque in the coronary arteries.

4.2.2 *Assessment of Coronary Plaques*

The radiologic report was used for classification of plaque buildup in the coronary arteries. The phase with highest reconstruction quality was selected and used to assess plaque development. Additional reconstructions in this phase were made using a B26f kernel, 0.6 mm slice thickness and 0.4 mm increment. For each segment the most obstructive plaque (i.e. highest degree of stenosis) was considered and assessed. The degree of stenosis was determined by the percentage of surface area filled with plaque. Plaque without lumen narrowing were categorized as 0% stenosis. Segments with lumen narrowing were categorized as <50% stenosis, 50-70% stenosis, or >70% stenosis (Figure 4.1). The assessed plaque was categorized as calcified, soft, or the mixed type. When multiple plaques were present in one segment, only the plaque with the highest degree of stenosis was assessed. When plaques with equal degree of stenosis were present in a segment, the longest plaque was assessed. Arteries were classified for degree of stenosis according to the most obstructive plaque.

The most obstructive plaque in a segment was assessed on CPR view (Figure 4.2). Cross-sections through the centerline were used to determine the location of the myocardium with respect to the vessel (Figure 4.3). The cross-section of the vessel was divided into four segments, starting with the segment 1_M most closely located to the myocardium and increasing numbers clockwise. Cross-sectional view was oriented from distal to proximal, corresponding with the 'classic anatomic view' from caudal to cranial. We defined that plaque was only located in a segment when it filled more than 50% of this segment, based on the cross-sectional view. Accordingly, when a segment was clearly curved at the location of the most obstructive plaque, the inner curve segment ($1_{IC} - 4_{IC}$) was defined. It was also reported when no myocardium or inner curve segments could be designated. Distribution of plaque into four segments with

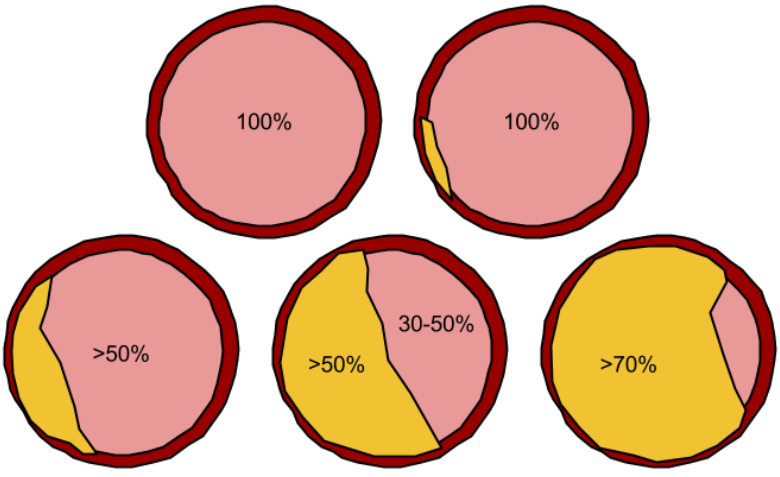

Figure 4.1: Schematic transverse views of plaque stenosis classification used in this study. Percentages placed in the pink area represent the remaining lumen and in the yellow area the amount of stenosis as percentage of the total lumen proximal from the plaque.

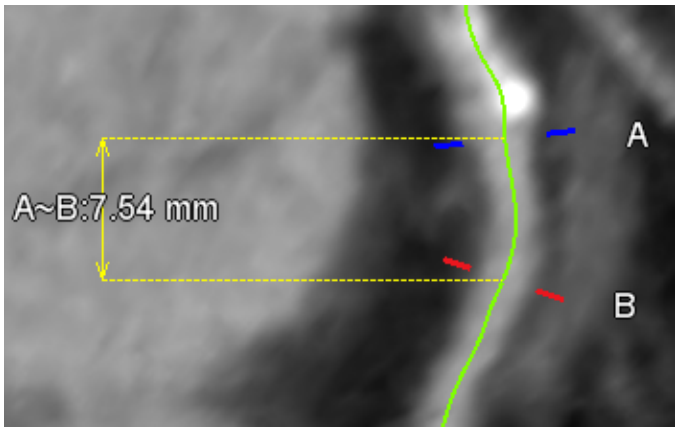

Figure 4.2 Example of plaque analysis measurement in the mid-LAD with <50% stenosis. Soft plaque is visible between the red and blue markers with a total length of 7.5 mm, and has a connection with the proximal segment.

respect to the inner curve was reported similarly as for the myocardium. 3D volume rendered images were used to assist in site orientation to categorize the plaque (Figure 4.3). Segment 1_M and 1_{IC} can be rotated in relation to each other.

Each plaque that extended beyond the boundaries of a segment was assigned to the segment containing the most obstructive part, or when this could not be determined, the longest part of plaque. Length of the plaque was measured and used to calculate the percentage of a segment filled with plaque. Plaque percentage was corrected for plaques covering multiple segments. This was done by including the length of every segment the plaque spanned in the total segment

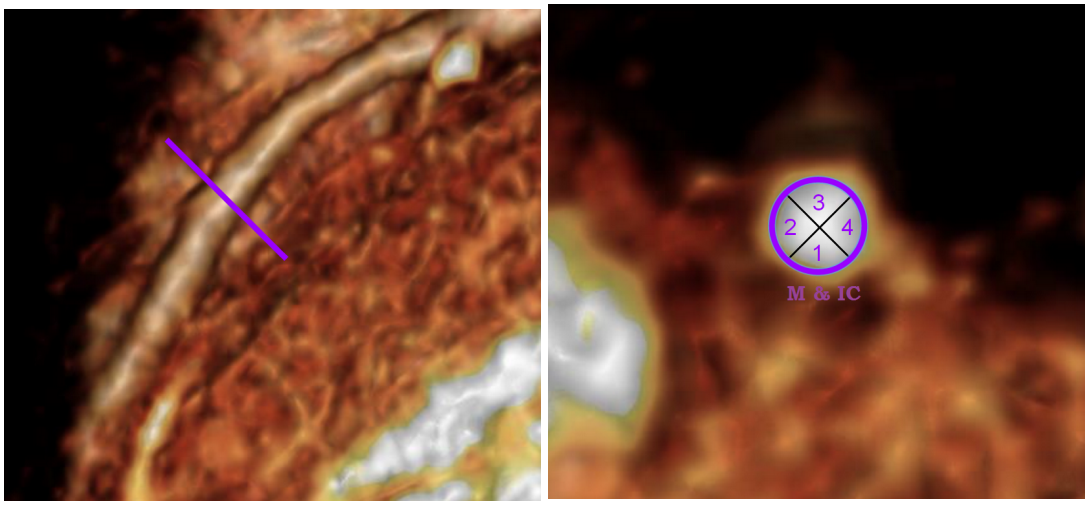

(a) Part of an LAD that is bent along the myocardium. Cross-section is made at the purple line. This information is used in inner curve segmentation.

(b) Cross-sectional view at level of the purple line. The myocardium is shown beneath the vessel. Combined with 3D information from **(a)**, segment 1_M and 1_{IC} are aligned.

Figure 4.3 Myocardium and inner curve segmentation. Rotation of both segmentations are equal (i.e. $1_M \sim 1_{IC}$) in this image since this vessel is bent along the myocardium in a normal way.

Table 4.1: Overview of characteristics assessed during plaque analysis.

Plaque parameter	Parameter measured / option
Degree of stenosis	0%, <50%, 50-70%, >70%, 100% (Figure 4.1)
Type of plaque	Calcified / soft / mixed
Plaque length (mm, %)	Millimeters are variable; percentage between 0-100%
Passage with segments	No connection / with proximal / with distal
Myocardium segment	Myocardium site is defined as 1; Yes (1) or no (0) for all four segments
Inner curve segment	Inner curve is defined as 1; Yes (1) or no (0) for all four segments

length. Plaque length remained the same in these cases. An overview of the assessed parameters for each most obstructive plaque in a segment is given in Table 4.1.

4.2.3 *Statistical Analysis*

Geometrical parameters were mutually tested with Pearson's product-moment correlation coefficient. Correlation was considered significant when $p<0.01$ (two-tailed). Linear mixed model's were applied to investigate associations between geometrical parameters and the degree of stenosis. These models account for multiple arteries or segments in an individual as repeated measures. Compound symmetry (heterogeneous or normal) covariance type was chosen by parsimony and based on Akaike's Information Criteria (AIC). In addition to geometric difference parameters (as described in Chapter 3), the average of ES and ED phases were also tested. Geometrical parameters were chosen as dependent variable in the model, to investigate possible interactions with arteries or segments. Degree of stenosis categories were dichotomized into no plaques and plaques with no lumen narrowing (LN negative group) versus plaques with lumen narrowing (LN positive), plaques with <50% stenosis versus plaques with >50% stenosis, and plaques with <70% stenosis versus plaques with >70% stenosis.

Associations of geometrical parameters with plaque type and length were investigated using linear mixed models. Plaque length is depicted as total length (in mm) or as percentage determined by the segment or segments length it spanned (in %). Estimated marginal means were used between groups in the linear mixed model depicting lumen narrowing, stenosis or plaque type. Unless stated otherwise, statistical p-values of <0.05 (two-tailed) were considered significant.

Related sample Cochran's Q tests were used to analyze distribution of plaque in the myocardium and inner curve segments. Bonferronized p-values were used for pairwise comparisons between groups. Since both myocardium and inner curve have four (k) segments (categories), the number of pairwise comparisons is six ($k * (k-1)/2$). We applied a Bonferronnization of

	Arteries	Segments
No plaque	23 (16.8%)	186 (40.8%)
0% stenosis	5 (3.6%)	51 (11.2%)
<50% stenosis	42 (30.7%)	101 (22.1%)
50-70% stenosis	18 (13.1%)	43 (9.4%)
>70% stenosis	49 (35.8%)	75 (16.4%)
Total	137 (100%)	456 (100%)

Table 4.2: Overview of plaque frequencies and percentages in artery and segment groups.

Table 4.3: Descriptive statistics of plaque characteristics in the segments group. The 186 (40.8%) segments that were free of plaque were not included in this table.

	0% stenosis	<50% stenosis	50-70% stenosis	>70% stenosis	**Total**
Type of plaque					
Calcified	47 (92.1%)	34 (33.7%)	19 (44.2%)	24 (32.0%)	124 (45.9%)
Soft	0 (0%)	34 (33.7%)	8 (18.6%)	8 (10.7%)	50 (18.5%)
Mixed	4 (7.8%)	33 (32.7%)	16 (37.2%)	43 (57.3%)	96 (35.6%)
Passage with segments					
No connection	43 (84.3%)	59 (58.4%)	23 (53.5%)	42 (56.0%)	167 (61.9%)
With proximal	5 (9.8%)	13 (12.9%)	8 (18.6%)	12 (16.0%)	38 (14.1%)
With distal	3 (5.9%)	29 (28.7%)	12 (27.9%)	21 (28.0%)	65 (24.1%)
Plaque length (mm)					
Mean (± sd)	3.4 (±1.5)	9.3(±5.1)	8.3 (±3.5)	14.9 (±6.4)	9.6 (±6.2)
Median [range]	3.1 [0.8 ; 6.9]	8.6 [2.2 ; 28.4]	7.6 [2.4 ; 15.0]	14.7 [2.2 ; 30.7]	8.3 [0.8 ; 30.7]
Total	**51 (18.9%)**	**101 (37.4%)**	**43 (15.9%)**	**75 (27.8%)**	**270 (100%)**

the previous p-value (0.05), resulting in a new p-value of 0.05 / 6 = 0.008. Myocardium and inner curve segments were analyzed on associations with geometrical parameters.

Interesting results were further analyzed by omitting plaques that had passage with other segments. The same was done by omitting the proximal RCA (segment 1) and LM (segment 5) from the analyses, to investigate the effects of only the segments closely located to the myocardium.

4.3 RESULTS

As mentioned before in Chapter 3, 137 (64.3%) from 213 arteries could be fully included and 456 (71.4%) from 639 segments. Table 4.2 depicts from these included arteries and segments the frequency of plaques for every category. There were 114 (83.2%) arteries and 270 (59.2%) segments with at least one plaque. Plaque type differentiation was performed only on segment level, which resulted in 124 (45.9%) segments with calcified plaques, 50 (18.5%) soft plaques, 96 (35.6%) mixed plaques, and 186 segments without plaque (40.8%). From the plaques, 167 (61.9%) were only found in one segment, where 38 (14.1%) plaques were connected with the proximal and 65 (24.1%) with the distal segment. Plaque characteristics on segment level for each degree of stenosis group are given in Table 4.3.

Table 4.4: Linear mixed model associations on artery level. Dependent variables (averages of and differences between ES and ED values) are depicted in the rows, factors in columns. LN- means group with no lumen narrowing, LN+ the group segments with lumen narrowing. EMM are estimated marginal means, with in parenthesis the standard errors. Significance is denoted with an asterisk.

Arteries	Degree of stenosis (dichotomized)					
	LN-	**LN+**	**<50%**	**>50%**	**<70%**	**>70%**
$\overline{Curvature}$ (mm^{-1})						
EMM	.071 (.004)	.076 (.002)	.072 (.002)	.079 (.002)	.073 (.002)	.079 (.003)
p-value	.218		.038*		.065	
$\overline{Tortuosity}$						
EMM	1.44 (.05)	1.40 (.02)	1.42 (.03)	1.40 (.03)	1.42 (.03)	1.39 (.04)
p-value	.505		.739		.518	
$\overline{Infl.\ points}$						
EMM	1.91 (.20)	2.12 (.10)	1.95 (.12)	2.22 (.13)	2.03 (.11)	2.17 (.15)
p-value	.328		.131		.433	
Δ *Curvature* (mm^{-1})						
EMM	.006 (.003)	.008 (.001)	.006 (.002)	.009 (.002)	.006 (.001)	.009 (.002)
p-value	.428		.142		.241	
Δ *Tortuosity*						
EMM	.057 (.012)	.036 (.006)	.035 (.007)	.046 (.008)	.039 (.007)	.042 (.009)
p-value	.098		.299		.785	
Δ *Infl. points*						
EMM	.11 (.13)	.27 (.07)	.16 (.08)	.31 (.08)	.24 (.07)	.23 (.10)
p-value	.281		.185		.913	

Table 4.5: Linear mixed model associations on segment level. Dependent variables (averages of and differences between ES and ED values) are depicted in the rows, factors in columns. LN- means group with no lumen narrowing, LN+ the group segments with lumen narrowing. EMM are estimated marginal means, with in parenthesis the standard errors.

Segments	Degree of stenosis (dichotomized)			
	LN-	**LN+**	**<50%**	**>50%**
$\overline{Curvature}$ (mm^{-1})				
EMM	.079 (.002)	.084 (.002)	.082 (.002)	.080 (.003)
p-value	.071		.603	
$\overline{Tortuosity}$				
EMM	1.11 (.007)	1.11 (.008)	1.11 (.006)	1.11 (.010)
p-value	.694		.736	
$\overline{Infl.\ points}$				
EMM	.54 (.05)	.60 (.05)	.55 (.04)	.63 (.07)
p-value	.395		.352	
Δ *Curvature* (mm^{-1})				
EMM	.006 (.001)	.008 (.001)	.007 (.001)	.008 (.002)
p-value	.279		.607	
Δ *Tortuosity*				
EMM	.019 (.003)	.016 (.003)	.018 (.002)	.017 (.004)
p-value	.440		.798	
Δ *Infl. points*				
EMM	.14 (.03)	.10 (.03)	.13 (.03)	.10 (.04)
p-value	.339		.624	

Table 4.6: Linear mixed model associations of plaque type and length at segment level. Dependent variables (averages of and differences between ES and ED values) are depicted in the rows, factors in columns. LN- means group with no lumen narrowing, LN+ the group segments with lumen narrowing. EMM are estimated marginal means, with in parenthesis the standard errors. Significance is denoted with an asterisk.

Segments	Plaque type			Plaque length	
	Calcified	**Soft**	**Mixed**	**In *mm***	**In %**
$\overline{Curvature}$ (mm^{-1})					
EMM	.080 (.003)	.084 (.005)	.083 (.003)		
p-value		.602		.023*	.010*
$\overline{Tortuosity}$					
EMM	1.11 (.009)	1.09 (.014)	1.11 (.010)		
p-value		.473		.553	<.001*
$\overline{Infl.\ points}$					
EMM	.67 (.07)	.50 (.10)	.64 (.08)		
p-value		.371		<.001*	<.001*
Δ *Curvature* (mm^{-1})					
EMM	.007 (.002)	.005 (.003)	.010 (.002)		
p-value		.427		.086	.814
Δ *Tortuosity*					
EMM	.018 (.004)	.015 (.006)	.020 (.004)		
p-value		.796		.036*	.001*
Δ *Infl. points*					
EMM	.17 (.05)	.11 (.07)	.06 (.05)		
p-value		.317		.449	.745

4.3.1 *Geometry Correlations*

On artery level, the number of inflection points showed a significant positive correlation with vessel length, curvature, and tortuosity (p<.001). Tortuosity showed also a significant positive correlation with vessel length (p<.001). These correlations were found in ES and ED phase. Mutual correlations between these parameters were stronger on segment level, where segment length, curvature, tortuosity, and the number of inflection points showed all significant correlations (p<.01) in ES and ED phase. Only segment length showed negative correlation with curvature (p<.001). Regarding differences of the geometrical parameters, only tortuosity was significantly correlated with artery length. On segment level the difference in tortuosity was significantly correlated with differences in curvature, segment length, and number of inflections points (p<.001), and the number of inflection points was correlated with curvature (p=.001).

4.3.2 *Linear Mixed Model Associations*

Results of the linear mixed models can be found in Table 4.4 (arteries) and Table 4.5 (segments). On artery level, only mean curvature was significantly associated with degree of stenosis when split at 50% (p=.038). Although not significant, increasing values were observed in estimated marginal means with more lumen narrowing for curvature and the number of inflection

points, and a negative trend for tortuosity. There were no significant predictors for geometrical parameters and no clear visual trends on segment level (Table 4.5).

Association results for plaque type and length are given in Table 4.6. None of the geometrical parameters were significantly associated with type of plaque. Multiple significant associations were found between plaque length and curvature (average), tortuosity (average and difference), and the number of inflection points (average).

Both plaque length and plaque percentage could be significantly predicted with the models by all dichotomized degree of stenosis categories ($p<.0001$). They were also able to significantly distinguish between all the original degree of stenosis categories ($p<.0001$). Observing estimated marginal means (with standard errors) for the corrected plaque percentage we found 11.1% (2.4%) for 0% stenosis, 28.2% (1.6%) for <50% stenosis, 24.9% (2.6%) for 50-70% stenosis, and 37.6% (1.8%) for the >70% stenosis group.

All the associations we found were even stronger when only plaques that were present in one segment were observed. Omitting the proximal RCA and LM had no or insignificant influence on the results.

4.3.3 *Myocardium and Inner Curve Segments*

An example of plaque distribution assessment with spatial relationship to the myocardium and curve of the coronary artery can be seen in Figure 4.4. The distribution of plaque with respect to the myocardium could be assessed in 236 (87.4%) of 270 segments. Distribution with respect to the inner curve could be assessed in 110 (40.7%) segments. Segments where no position towards the myocardium could be designated were mostly seen in the LM (30 segments, 11.1%). Distribution of plaque in myocardium and inner curve segments can be found in Figure 4.5. Cochran's tests were also performed for each of the pairwise comparisons, of which the results can be found in Table 4.7. In myocardium segment distribution, plaque was only more frequently found in segment 1_M versus segment 3_M ($p=.003$). Plaque was also more frequently found in segment 1_{IC} of the inner curve with respect to the other individual segments ($p<.001$).

Myocardium and inner curve were tested only with segment 1 as independent factor to predict geometrical parameters. Afterwards, combinations of all four segments were analyzed. Both analysis yielded no significant associations between one segment (nr. 1) or all segments with any geometrical parameters.

4.4 DISCUSSION

Geometry parameters (averages and differences) used for this part of the study were described in Chapter 3. Comparable studies about geometry quantification and corresponding limitations

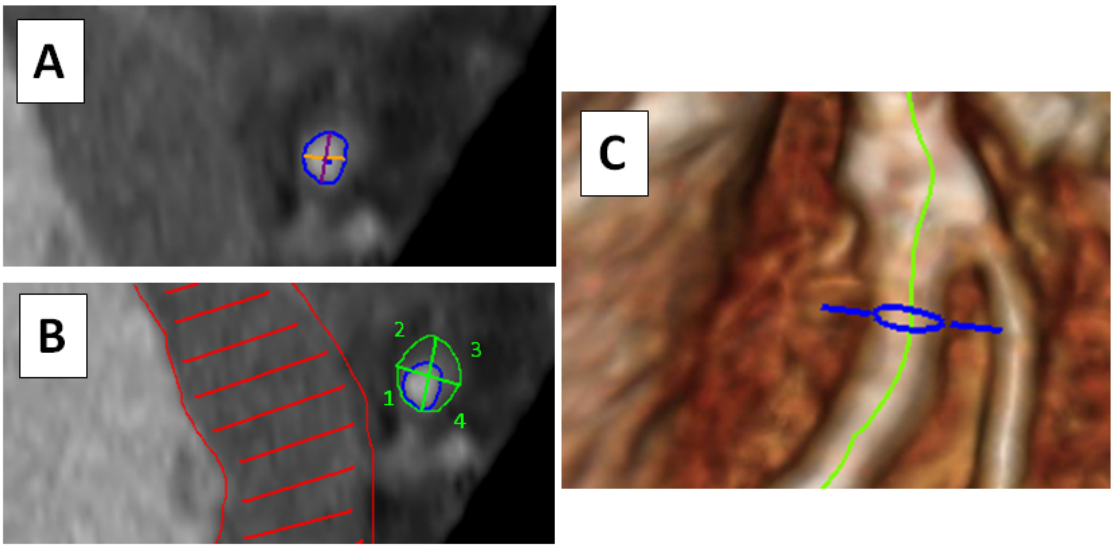

Figure 4.4 Same plaque as Figure 4.2. **(A)** Cross-section of the most obstructive part, **(B)** myocardium (red shaded) site defined, with plaque distributed in segments 2 and 3, **(C)** inner curve defined using 3D volume rendering. Plaque is distributed in segments 1 and 2.

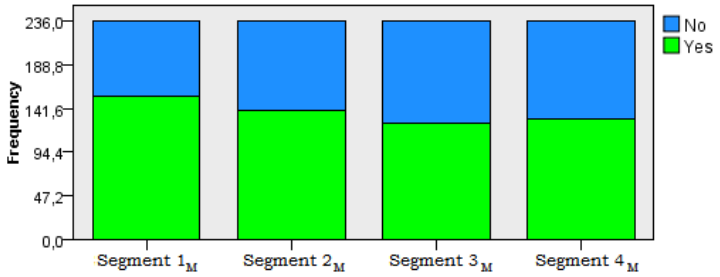

(a) Myocardium: with asymptotic significant distribution between all four sites (p = 0.017).

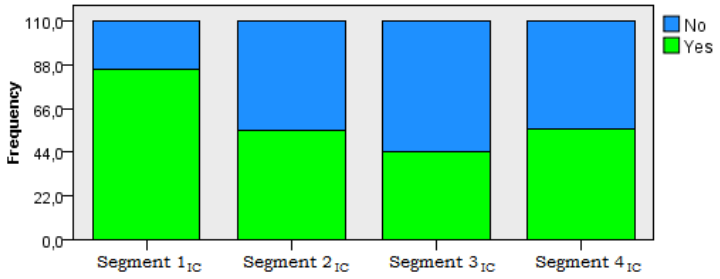

(b) Inner curve: with asymptotic significant distribution between all four sites (p<0.001).

Figure 4.5 Related-samples Cochran's Q tests and distributions in the four created myocardium and inner curve segments. 'Yes' represents presence of plaque and 'No' absence of plaque.

are discussed in previous chapters and not repeated here. The focus of this discussion will be on plaque development assessment and its association with dynamic coronary geometry. Most important issue addressed in this study was: How can hemodynamic preferred sites of coronary plaque development be quantified and how are they associated with previously determined (static and dynamic) geometrical parameters? Answering this question should eventually

Table 4.7: Pairwise comparisons according to Cochran's Q test. Significance is indicated with an asterisk when p<.008.

Segment X vs. Segment Y →	1 vs. 2	1 vs. 3	1 vs. 4	2 vs. 3	2 vs. 4	3 vs. 4
Myocardium (p-value)	.084	.003*	.013	.212	.442	.631
Inner curve (p-value)	<.001*	<.001*	<.001*	.172	.785	.101

lead to an advice for clinicians whether they should consider coronary artery geometry in CAD assessment and how. The results showed that previously determined static and dynamic parameters are not associated with degree of stenosis in the current dataset. Only plaque length can be related to both stenosis and geometry of the coronary arteries.

We tried to reproduce our findings from Chapter 2 although other data, patient groups, and parameters were used. Previously, we found that curvature and tortuosity are suitable geometrical predictors on artery and segment level of plaque presence and hemodynamic significant stenosis based on >70% lumen narrowing. This study showed only slight significant association between (average) curvature with groups of <50% and >50% stenosis on artery level. These results conflict with the previous results from the static study based on the same parameters. However, we can designate two main determinants in both studies that may contribute to different results.

First, patient groups as described in method sections of Chapter 2 (static study) and Chapter 3 (dynamic study) are substantially differing in patient inclusion. Patients from the GROUND-2 study [25] were recruited when they had symptomatic extra-cardiac arterial disease, but no history or complaints of symptomatic CAD. Patients from the dynamic study were included mostly from the CARDUCCI study (52 of 71 patients, 73.2%),[53] 7 (9.9%) from the TACS study,[55] and 12 (16.9%) from the GROUND study.[54] In contrary, the CARDUCCI study included patients that were scheduled for ICA and TACS included patients with acute chest pain. Based on these selections, the patient group used in the dynamic study are on average more severe cases of CAD, where the GROUND-2 study even included patients with no cardiac disease at all. Our hypothesis is that patients more severely affected by CAD have undergone (more) geometry changes. Besides, hemodynamics have altered in these patients due to plaque build-up in the arteries, which may lead to even more sites of plaque development. This possible explanation remains to be tested, for instance by carefully selecting and investigating patients with multiple degrees of disease (see also subsection 5.1.4). We also observed that semi-automatic centerline extraction was more difficult in patients with severe CAD. This may have hampered accuracy of geometry assessments. Further demographics like number of inclusions, age, and gender were comparable between the patient groups.

Second, data used in both studies differed in reconstruction parameters. The static study quantified geometry on slices reconstructed as consecutive 0.6 mm slices, whereas the dynamic study used thicker slices of 2.0 mm. The intended use of these 'thick slices' was originally to select the phase with least motion artifacts, to reconstruct 'thin slice' data of 0.6 mm. Data

used for extraction coronary centerlines in clinical CAD assessment usually has a resolution of 0.4 mm (slice interval and pixel spacing), which is also maintained by Schaap *et al*. in their evaluation framework for coronary centerline extraction algorithms.[64] Our multi-phase data in the dynamic study has an average slice interval of 2.0 mm and pixel spacing of 0.85 mm. It is obvious that these resolution characteristics yield less accurate geometry measurements, but its exact influence is yet unknown. To investigate the influence of different reconstruction thicknesses, a subset of patients should be investigated on both consecutive slices of 0.6 mm and 2.0 mm.

Our results suggest that differences in curvature, tortuosity, and number of inflection points cannot be associated with or predict preferred sites of plaque development. Since this is the first study to our best knowledge investigating the direct association of dynamic coronary geometry with quantified plaque parameters without applying CFD, it is hard to compare results with other studies investigating similar issues. CFD studies were incentive for this research, where sites of low WSS were linked with coronary geometry.[6, 14, 16, 19, 20, 46, 47] However, some studies also suggested that dynamic geometry characteristics are not always represented or influenced by shear stresses in certain segments.[49, 50] A comparison between certain studies and our study is especially hard to achieve considering the large amount of variability between those studies. Examples of factor contributing to this variability are: the assessed segments or arteries, which (recent) imaging techniques were used, patient or model-based analysis, which variables/parameters were measured, and which mutual relations between geometry, hemodynamics, or plaque development were described or studies. Therefore, our study tried to directly relate static and dynamic coronary geometry of all (large) arteries and segments with plaque development based on cCTA imaging.

An interesting similarity with most CFD studies was that we were also able to locate most of our plaques located in the inner curve of vessels.[17] Furthermore, a comparable method was applied with IVUS technique by Iwami *et al.*, who found preferential sites of atherosclerosis along the inner arc of coronary vessels.[20] We showed that this can be measured with cCTA imaging, but is still not associable with coronary geometry. If geometrical parameters can be used to 'recognize' certain segments where plaques develop along the inner curve, it could be used as potential risk factor for developing CAD. Furthermore, the inner curve segment could only be designated in 40.7% of the cases on cCTA, and assessment was rather subjective. IVUS would be a better distribution tool, as performed by [20] *et al.* This technique can achieve resolution of 100-150 μm[65] which makes is possible to determine the percentage of plaque in each cross-sectional segment, rather than depicting whether plaque is present or not in a segment like in our method. The limitations of the proposed plaque distribution method demonstrate that this method should be improved on many aspects and is still far from clinical practice.

An option is to obtain more localized curvature values. However, the disadvantage is that this would be hard to generalize among patients. Landmarks that could always be identified (like side branches) should be used to compare parts of coronary arteries among individuals.

Observing the site of maximum curvature in a vessel can also be an option worth to investigate, but CFD studies like the study from Johnston *et al.* show that lowest (and highest) WSSs not appear on the maximum bend of a vessel, but slightly behind the curve. This observation is explained by the definition of wall shear stress (see section 1.2 and Equation 1.1), which is dependent on the blood velocity gradient at the vessel wall. Driven by its kinetic energy, blood tends to move straight ahead in vessels, which results in less particles (and less flow) at the vessel wall behind a curve.

The only relevant associations that were found in this part of the study were between multiple of our parameters and plaque length or percentage on segment level (Table 4.6). This plaque length and percentage were strongly associated with lumen narrowing ($p<.0001$) as defined in four categories. However, this measure is currently of no use in clinical practice, where based on cCTA significant stenoses are assessed by the degree of lumen narrowing as a result of coronary plaque. Our geometrical parameters could not be directly related to the degree of stenosis, which was the initial purpose of this study. Based on this findings, our parameters are not defined well enough and should be adapted more to accommodate hemodynamic deviating situations in the coronary arteries. Furthermore, it should be noted that the degree of lumen narrowing based on cCTA is a moderate parameter in assessing hemodynamic significant stenoses, which is ideally based on functional information like myocardial perfusion.[66] Thus, parameters like plaque length or percentage are even further away from functional information about myocardial functioning.

Limitations of centerline extraction, which frequently required manual interference, has been mentioned before in this study. Regarding our plaque analysis, centerline extraction was especially hard in patients with severe forms of CAD. The high number of exclusions is mainly caused by this patient group, where the most affected arteries had to be excluded. For instance, patients with complete obstruction of an artery were not included in this study, but certain cases were encountered. This can be considered as selection bias in the study. However, we stated before that differences between our results from the static and dynamic studies may be explained by different degrees of hemodynamic alterations in more affected patients. Besides, patients with severe CAD often demonstrated signs of forming of collaterals. These cases were also excluded from this study due to abnormal hemodynamic situations, which also contributes to the selection bias.

It can be summarized that the associations we found in this study are still too weak to have clinical relevance. It is recommended to overcome the mentioned limitations and to improve this research on their discussed aspects. Furthermore, the next chapter (Chapter 5) will elaborate more upon possibilities for future directions in this field of research. Based on the findings from this study, the most important recommendation would be to investigate or improve geometrical parameters such that they would better reflect hemodynamic deviations in the coronary arteries.

CHAPTER 5

General Discussion and Conclusion

5.1 FUTURE DIRECTIONS

Throughout this work multiple limitations have been revealed of the performed (sub)studies and options have been given to further improve research towards the potential of coronary geometry as an imaging biomarker. This has been accompanied by ideas that are potentially interesting to investigate. Some of these ideas have already been implemented in the current study, whereas others have not. A number of those not yet implemented ideas were not the most obvious choice to study or were far-fetched at first glance, but they do have an interesting potential and should be considered. Therefore, the following sections will elaborate upon these topics, and provide possible future directions in this area of research.

5.1.1 *Alternative Geometrical Parameters*

In the work described in this report multiple geometrical parameters were quantified on CT datasets. Main geometry quantifiers were curvature and tortuosity, which are common geometry describing parameters for the coronary arteries, as has already been discussed in Chapter 2 and Chapter 3. Furthermore, the number of inflection points has been introduced to represent the 'winding' aspect (static parameter) and compression of the vessel or segment (dynamic parameter). Curvature and tortuosity were also mainly chosen for simplicity, since these parameters were embedded in the same software used to analyze the datasets and extract centerlines of coronary arteries. In Chapter 2 we found some significant associations between these parameters and the severity of coronary stenosis. However, Chapter 4 showed that these results appear less robust and perhaps apply only on specific patient groups or require data with sufficient image quality for the measurements. Therefore, our chosen parameters are not ideal in predicting or being associated to coronary plaques. More descriptive parameters that correspond to hemodynamic alternative situations should be considered.

The goal of ideal geometric parameters that could serve as imaging biomarkers would be to describe associations with aspects of CAD. Although we were limited by the parameters embedded in our software, it was possible to extract and transfer coronary centerlines in an

interactive environment for numerical computation and visualization.[1] Figure 5.1 shows examples of extracted RCAs in end-systolic and end-diastolic phases. A more accurate geometrical parameter for the coronary arteries can be designed, that ideally takes into consideration that coronary arteries always follow a three-dimensional trajectory due to the shape of the heart. The normal anatomic path a coronary artery is supposed to follow can be considered as a reference. Alternative coronary geometry that may lead to hemodynamic alterations should be based on deviations to its intended course. However, while centerlines through coronary arteries can be extracted with threshold-based algorithms, defining the 'normal' course of the coronary arteries based on the outer surface of the myocardium and the grooves between heart chambers adds complexity. An option is to fit a polynomial plane to represent the curved myocardium surface (Figure 5.2). Based on this, it is theoretically possible to extract parameters describing the deviation from this plane.

Another possibility is to extract multiple centerlines of coronary arteries in an environment as Figure 5.1 and Figure 5.2. By carefully selecting the appropriate group of patients with equal or comparable severity of CAD, a 'coronary atlas' could be constructed. However, it seems hard to select a representative sample of patients for this purpose, since the process of plaque development may already be ongoing but undetected, thus hampering the selection of 'healthy' vessels to be included in the atlas model. Furthermore, coronary arteries exhibit large variability in length, shape, size, amount of movement during the cardiac cycle and possibly more factors, which is disadvantageous for building a normal model.

5.1.1.1 *Disadvantages of Alternative Geometry Analysis*

From the preliminary analysis resulting in the previous mentioned images, another disadvantage of investigating other geometrical parameters or even our current method pops up. In the multiphase images of Figure 5.1a, it can be observed that the origin of these RCAs is not located at a similar point. Although a beating heart may result in (slight) movement of the origin, it is the question whether the difference can be as big as in this image, or if this resulted from reconstruction artifacts. Lu *et al*. quantified coronary motion on electron-beam tomography images and maintained a reasonable velocity criterion of 35 mm/s for the RCA.[67] However, criterion is based upon measurements of the middle portion of the RCA and this refers to velocity, instead of motion range. It remains an important issue whether arteries in multiple phases should be translated to a same origin (Figure 5.1b) or not, and it should be carefully considered when certain analyses will be performed. Our observation could also be an explanation why geometrical differences in our study showed no associations with CAD.

We discussed in this section that it could be possible to obtain alternative geometry measures, but creating sufficient sample sizes to obtain significant results will theoretically be hard to achieve. Furthermore, modeling of the 'default' trajectory of the coronary arteries is accompanied

[1] MATLAB® by MathWorks. http://nl.mathworks.com/.

by making assumptions that cannot always represent the actual situation. Our research was set-up as simple as possible, but this analysis will just like CFD studies correspond less to reality.

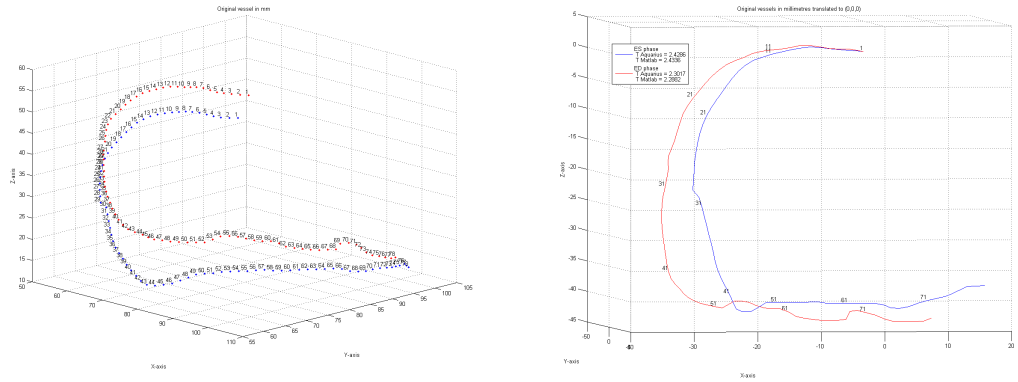

(a) The ES (blue) and ED (red) phases of an RCA depicted as individual points.

(b) The ES (blue) and ED (red) phases with measurements and begin points translated to a shared origin.

Figure 5.1 Examples of extracted RCAs centerlines of one patient in ES and ED.

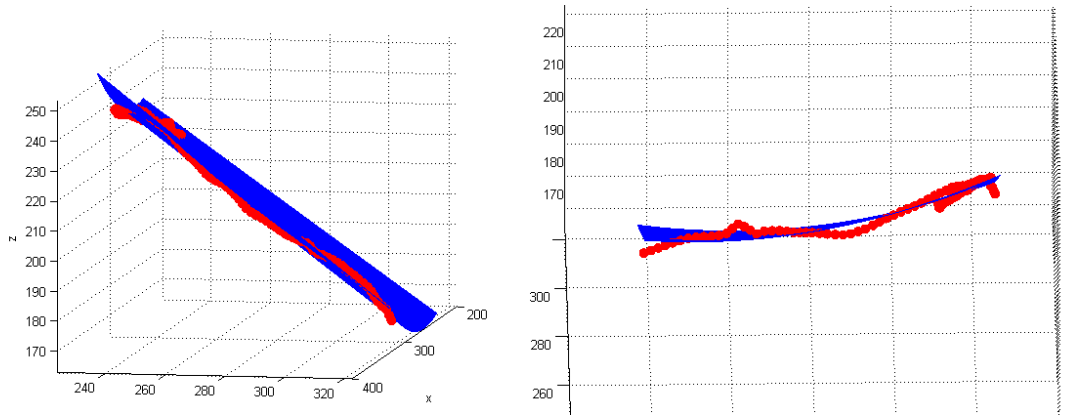

(a) Side / front view.

(b) Side view.

Figure 5.2 Examples of an extracted RCAs centerline with fitted polynomial plane. Centerline is depicted in red, and polynomial plane in blue.

5.1.2 *Coronary Centerline Extraction Validation*

Throughout this study the automated coronary centerline extraction method from the Aquarius iNtuition software from TeraRecon was used (subsection 1.1.3 and method sections for reference). All geometrical measurements were based on the extracted centerlines with this software. However, there are more software packages from vendors that can provide post-processing tools for coronary imaging, but obviously are based on other algorithms. It is interesting to investigate how different software competitors score on this component. Schaap *et al.* developed a standardized evaluation methodology for evaluating coronary artery centerline extraction

algorithms.[64][1] They already evaluated 23 coronary artery centerline extraction methods with their framework based on reference and testing data. Our software with embedded extraction algorithm is considered visually sufficient enough and widely used in the clinic setting for coronary CT imaging. However, it was noted that manual adjustment of the centerline was often required, especially in areas involved in coronary artery disease with plaques and calcifications present. These adjustments could have major impacts on geometrical measurements, making it extremely important that this was performed equally in both phases of one patient. Equivalent adjustment between individuals was more difficult. Some centerlines were visually extracted almost perfectly, whereas some required much manual adaptations.

It would be interesting to test the used extraction algorithm with the evaluation framework developed by Schaap *et al*. However, our research focused on geometrical measurements. A coronary centerline extraction validation that also validates geometrical measurements of the centerline would be even better. For example, this can be performed using a (dynamic) phantom representing coronary arteries with different levels of calcifications. Information about calcifications and geometry can be based on the phantom manufacturing, which can be used in validation of our method. However, it would be hard to produce a phantom that realistically simulates the in vivo situation. Respiratory and cardiac motion (with possible irregularities), ECG registration, and signal attenuation by extra-cardiac tissue are examples of factors that can influence the quality of the eventual geometrical measurements. These factors should clearly be considered when performing a phantom study on coronary geometry.

Created centerlines are often visualized with CPR to assess coronary lumen on plaques and/or stenoses (Figure 1.5). A main limitation is that CPR methods are always dependent on the quality of the computed central axis (i.e. centerline), and that only parts of vascular structures that are touched by the re-sampled surface are visible on the CPR view. Therefore, the promises and pitfalls of CPR are important to be kept in mind, since it may have major influences on the outcomes of this research. This point is only important in the visualization process to enhance luminal information of the coronary arteries and thus logically dependent on the quality of the extracted centerline. It should be noted that only the number of inflection points is based on the CPR. Vessel length, curvature, and tortuosity measurements are based on 3D plots of the centerlines and thus independent of CPR.

5.1.3 *Inter- and Intraobserver Variability*

An adequate inter- and intraobserver variability is required when geometrical measurements should eventually be taken into clinical routine. In Chapter 2 we measured these values (Table 2.3). Although sufficiently low variability was achieved for curvature and tortuosity measurements, still many improvements can be made for 'troublesome' segments and arteries

[1] The Rotterdam coronary artery algorithm evaluation framework. Accessible at coronary.bigr.nl.

like the LM and (segments of) the LCx. However, these values were obtained from geometrical measurements in the ED phase only. This phase (usually between 75-80% of the cardiac cycle) is also the most frequently assessed phase for CAD assessment in clinical practice, because of the least expected motion of the coronary arteries.[68] Considering dynamics of coronary geometry, the ES phase should also be assessed with corresponding variabilities. The coronary arteries are usually more in motion at this point of the cardiac cycle, which is the reason that the ED phase is more often used in clinical practice. In our clinic, ES phase is only scanned and reconstructed if ED reconstruction shows coronary assessment complicating artifacts, or if there is high prior probability that ED reconstruction only will not be sufficient enough. Therefore, inter- and intraobserver variability should be examined in multiple phases of the cardiac cycle, to use dynamic geometrical properties of the coronary arteries in future research. It is expected that those variabilities will be worse than the values for the ED phase found in this research, due to the hard assessable character of the ES phase.

5.1.4 *Time Evaluation of Dynamic Geometry*

An important issue that could not be resolved in this study, was the question whether changing coronary geometry through the cardiac cycle would be associated with plaque development, or if and to what extent coronary plaques would induce deviating geometry. It is most likely that geometry and CAD do not exhibit a simple cause-effect relationship. Both deviating coronary geometry and presence of coronary plaques are often both present and may reinforce each other. The term deviating coronary geometry complicates this issue even more. Based on this research, coronary geometry can only be quantified with parameters, and not be designated as deviating enough to give rise to coronary plaques. Furthermore, risk factors such as age, gender, and hypertension are cohesive for both coronary geometry and coronary plaques. Therefore, it may be hard to investigate and determine who the culprit and victim are in the coronary system, based on single-time observations and regarding the presence of numerous risk factors that can account for both parties.

The most basic thing to investigate, would be a (mature) arterial configuration in a healthy situation. When this geometry configuration is used as a starting or reference point, further follow-up can determine whether geometry has changed. This also brings along the technical challenge to scan and reconstruct coronary arteries of a subject in an equivalent phase when the subject is followed over time. Many determinants from image acquisition and post-processing may influence geometrical measurements. Examples are ECG registration, adequate reconstruction quality as in the first assessed phase, need of the same CT scanner, and comparable implementation of the centerline-extraction algorithm. Furthermore, adding the dynamic dimension of moving coronary arteries during the cardiac cycle would complicate this research even more. In order to investigate time-development of coronary artery geometry, the challenges of

doing so should therefore first be carefully considered and surmounted. As far as known, there are no present patient studies that followed a group patients over time to investigate the change of coronary geometry and its potential effects.

When possibilities for such a study arise, it may be interesting to observe patient without history of any arterial disease (i.e. healthy subjects) as stated before. For coronary imaging, CT is the current clinical assessment technique, but it is stated that neither cCTA nor MR angiography should be used to screen for CAD patients who have no signs or symptoms suggestive for CAD.[8] As mentioned before in Chapter 1, MR techniques are currently inferior on spatial resolution, consistency, examination time, and availability compared to CT. However, the major disadvantage of CT is that it uses ionizing radiation, making disease-free studies especially hard based on ethical issues. For example, patients from the dynamic study in Chapter 3 received an average dose of 22.5 mSv (±4.9 mSv), where background radiation in the Netherlands is on average 2.4 mSv each year.[1] In order to further study coronary geometry on cardiac healthy patients/subjects, its potential as imaging biomarker for CAD has to be demonstrated better and radiation exposure needs to be drastically reduced. Current generation CT scanners may overcome or improve the latter issue.

5.1.4.1 *Generations of Coronary CT Imaging*

The current coronary imaging modality in the UMCG is a first generation DSCT scanner (Somatom Definition AG, Siemens Medical Systems, Forchheim, Germany). This system was installed in May 2006 and used as imaging modality in this research. As stated in subsection 5.1.4, patients were exposed to comparatively high levels of radiation, especially those involved in the dynamic coronary geometry study. Next generations of DSCT scanners have developed and are implemented in clinical practice more and more. An overview of the latest generations DSCT scanners used for coronary imaging and relevant features are given in Figure 5.3 and Table 5.1. The UMCG will install Siemens's third generation DSCT scanner (Force) in the beginning of 2015 at the radiology department. Improvements of this scanner also pave the way for future coronary geometry investigations. Major advantages of the Force are the improved temporal resolution of 66 ms and the possible reduced radiation exposure of less than 0.4 mSv. Although our used algorithm for centerline extraction and corresponding geometrical measurements was not validated, improved temporal and spatial resolution of the Force could yield more accurate centerlines and be less sensitive for calcifications. Thus, geometrical measurements are more reliable and should have improved intra- and inter-observer variabilities. Installation of a third generation Siemens DSCT Force scanner (Figure 5.3b) next year in UMCG with possible radiation doses ot patients below 1 mSv can also create opportunities to perform studies with healthier subject groups (see subsection 5.1.4). However, there will be still radiation exposure and it remains the question whether medical ethical committees would allow studies to investigate

[1] Source: http://www.rivm.nl/Onderwerpen/S/Stralingsbelasting_in_Nederland

(a) SOMATOM® Definition Flash. **(b)** SOMATOM® Force.

Figure 5.3 Latest two generations SOMATOM® DSCT scanners by Siemens. Images from http://www.healthcare.siemens.nl/computed-tomography/.

Table 5.1: Features of three generations SOMATOM® Siemens CT scanners. Scan time and effective dose are stated for what is approximately possible in cCTA with prospective ECG-triggering. Information is derived from [53], [69] and http://www.healthcare.siemens.nl/computed-tomography/dual-source-ct.

	SOMATOM Definition	**SOMATOM Definition Flash**	**SOMATOM Force**
Generation DSCT	1^{st}	2^{nd}	3^{rd}
Acquired slices	128 (2 x 64)	256 (2 x 128)	384 (2 x 192)
Temporal resolution	83 ms	75 ms	66 ms
Spatial resolution	0.4 mm	0.30 mm	0.24 mm
Scan time	~8 s	~0.28 s	~0.2 s
Eff. dose	~2-4 mSv	~0.4 mSv	~0.3 mSv

certain groups of CAD-free patients with this newest generation DSCT imaging. Furthermore, when dynamic geometrical information about the coronary geometry needs to be obtained using retrospectively ECG-gating, the effective dose will increase and possibly be more than 1 mSv again.

5.1.5 *Geometry in the Human Arterial System*

In this work only the coronary arteries were considered and the influence of their geometry on CAD. A main reason for this focus is large prevalence of CAD patients and the associated risk of mortality. Furthermore, coronary arteries are the only vessel that are a life-time in motion, which influences hemodynamics that potentially triggers plaque development even more. However, other human arteries can be considered and quantified in geometrical terms as well. The implemented tortuosity measurements originally had their purpose at aortic bifurcation level.[28, 70] Furthermore, not only stenoses and plaque development are associated with hemodynamic parameters like the WSS, but also vessel aneurysms and in-stent re-stenoses are related before with deviating hemodynamic situation with respect to 'normal situations'.[13] Interesting parameters to investigate would be the carotid arteries for stenosis assessment,

vessels in the circle of Willis or the abdominal aorta for aneurysm development, or patients with coronary artery bypass grafts to assess re-stenosis. The dynamic part of Chapter 3 in this study can even be translated to frequently moving arteries located at joints, for example in popliteal artery stenosis. A major advantage would be that complicating factors like cardiac and respiratory motion are eliminated. Obviously, anatomy of vessels has to be accurately quantified by (other) geometrical parameters to represent a normal hemodynamic course of the vessel. Our curvature, tortuosity and inflection points parameter implementations are perhaps not most suitable for the coronary arteries (see subsection 5.1.1). Optimal geometrical parameters must account for deviations in hemodynamics that can lead to vessel wall weakening (aneurysms) or wall damage with thrombosis (stenosis), and should therefore be individually adapted to any type of blood vessel.

5.2 SUMMARY AND GENERAL CONCLUSION

In Chapter 2 the relationship between coronary artery geometry and the presence of coronary plaques was assessed using non-invasive coronary CT angiography (cCTA). This study demonstrated that curvature and tortuosity of the coronary arteries can be obtained using semi-automatic analysis of cardiac CT datasets with high inter- and intra-observer correlation. There is a relationship between the curvature of the coronary arteries and the presence of significant stenosis and/or plaque in the arteries. These findings provide a preliminary indication that coronary artery geometry could be a potential imaging biomarker for risk assessment of coronary artery disease.

Chapter 3 proposed a robust and valid method that can be used to quantify changing geometry of the coronary arteries during the cardiac cycle on retrospectively ECG-gated cCTA datasets. Curvature, tortuosity and inflection points measures were significantly higher in end-systole compared to end-diastole for coronary arteries as well as individual segments. These findings could be used to further investigate whether coronary artery geometry based on routine cCTA can identify preferential sites for plaque development.

The extent of CAD was quantified in Chapter 4 based on hemodynamic preferred sites of plaque development on the same dataset as used in the previous chapter. Our static geometry parameters are less robust then previously assumed based on the results in the second chapter. Dynamic geometry parameters yielded no significant association with degree of stenosis as well. However, both static and dynamic parameters were strongly associated with plaque length and percentage, which are in turn positively correlated with coronary stenosis on multiple levels. cCTA can also be used to determine cross-sectional distribution of coronary plaque which corresponds with hemodynamic findings, but plaque distribution was not associated with the quantified parameters. More specific geometry parameters should be designed that can directly associate with degree of coronary stenosis.

Finally, the current chapter (Chapter 5) provided some future perspectives to improve or expand the current research. The most interesting and first step should be to focus on improving geometrical parameters that better corresponds to the coronary hemodynamic situation and that can be associated with plaque development. Latest generation DSCT scanners can extend research through better temporal and spatial resolution, which should result in improved intra- and inter-observer variabilities and improved (validated) centerlines. When the potential of (dynamic) coronary geometry as imaging biomarker for CAD has been demonstrated thoroughly, the purpose of time-evaluation studies to reveal more about cause-effect relationship can be considered. With the current state of coronary geometry research, many steps needs to be taken and limitations to overcome, to eventually use coronary geometry as a risk factor for CAD in clinical practice.

In conclusion, the investigated static parameters are associated with plaque development. This association is not generalizable and depends on image quality and patient population. Dynamic parameters can be used to quantify movement of coronary arteries and segments. Both static and dynamic parameters are associated with length of plaques in coronary arteries, but not with the extent of stenosis. In the current state of research, our investigated parameters can not be used in predicting or associating with preferred sites of coronary artery disease. However, the current results do provide new and deeper insights in the anatomy, motion and deformation of the coronary artery tree and could eventually lead to the development of novel image biomarkers to identify risk of CAD.

Bibliography

[1] W. G. Austen, J. E. Edwards, R. L. Frye, G. G. Gensini, V. L. Gott, L. S. Griffith, D. C. McGoon, M. L. Murphy, and B. B. Roe, "A reporting system on patients evaluated for coronary artery disease. Report of the Ad Hoc Committee for Grading of Coronary Artery Disease, Council on Cardiovascular Surgery, American Heart Association," *Circulation*, vol. 51, pp. 5–40, Apr. 1975. (Cited on pages 1, 11, and 21.)

[2] D. M. Fiss, "Normal coronary anatomy and anatomic variations," *www.appliedradiology.com*, no. January, pp. 14–26, 2007. (Cited on page 2.)

[3] A. Hamdan, P. Asbach, E. Wellnhofer, C. Klein, R. Gebker, S. Kelle, H. Kilian, A. Huppertz, and E. Fleck, "A prospective study for comparison of MR and CT imaging for detection of coronary artery stenosis.," *JACC. Cardiovascular imaging*, vol. 4, pp. 50–61, Jan. 2011. (Cited on pages 2 and 61.)

[4] V. L. Roger, A. S. Go, D. M. Lloyd-Jones, E. J. Benjamin, J. D. Berry, W. B. Borden, D. M. Bravata, S. Dai, E. S. Ford, C. S. Fox, H. J. Fullerton, C. Gillespie, S. M. Hailpern, J. A. Heit, V. J. Howard, B. M. Kissela, S. J. Kittner, D. T. Lackland, J. H. Lichtman, L. D. Lisabeth, D. M. Makuc, G. M. Marcus, A. Marelli, D. B. Matchar, C. S. Moy, D. Mozaffarian, M. E. Mussolino, G. Nichol, N. P. Paynter, E. Z. Soliman, P. D. Sorlie, N. Sotoodehnia, T. N. Turan, S. S. Virani, N. D. Wong, D. Woo, and M. B. Turner, "Heart disease and stroke statistics–2012 update: a report from the American Heart Association.," *Circulation*, vol. 125, pp. e2–e220, Jan. 2012. (Cited on pages 2, 9, and 19.)

[5] M. Malvè, A. M. Gharib, S. K. Yazdani, G. Finet, M. A. Martínez, R. Pettigrew, and J. Ohayon, "Tortuosity of Coronary Bifurcation as a Potential Local Risk Factor for Atherosclerosis: CFD Steady State Study Based on In Vivo Dynamic CT Measurements.," *Annals of biomedical engineering*, July 2014. (Cited on pages 3, 5, 17, 19, 26, 27, and 61.)

[6] A. Wahle, J. J. Lopez, M. E. Olszewski, S. C. Vigmostad, K. B. Chandran, J. D. Rossen, and M. Sonka, "Plaque development, vessel curvature, and wall shear stress in coronary arteries assessed by X-ray angiography and intravascular ultrasound.," *Medical image analysis*, vol. 10, pp. 615–31, Aug. 2006. (Cited on pages 3, 5, 9, 16, 17, 19, 26, 31, and 41.)

[7] G. J. Pelgrim, M. Oudkerk, and R. Vliegenthart, "Computed Tomography Imaging of the Coronary Arteries," in *What Should We Know About Prevented, Diagnostic, and Interventional Therapy in Coronary Artery Disease*, InTech, 2013. (Cited on page 4.)

[8] D. A. Bluemke, S. Achenbach, M. Budoff, T. C. Gerber, B. Gersh, L. D. Hillis, W. G. Hundley, W. J. Manning, B. F. Printz, M. Stuber, and P. K. Woodard, "Noninvasive coronary artery imaging: magnetic resonance angiography and multidetector computed tomography angiography: a scientific statement from the american heart association committee on cardiovascular imaging and intervention of the council on cardio," *Circulation*, vol. 118, pp. 586–606, July 2008. (Cited on pages 4 and 48.)

[9] C. Yutani, M. Imakita, H. Ishibashi-Ueda, Y. Tsukamoto, N. Nishida, and Y. Ikeda, "Coronary atherosclerosis and interventions: Pathological sequences and restenosis," *Pathology International*, vol. 49, pp. 273–290, Apr. 1999. (Cited on pages 4 and 9.)

[10] W. J. Manning, R. Nezafat, E. Appelbaum, P. G. Danias, T. H. Hauser, and S. B. Yeon, "Coronary magnetic resonance imaging.," *Cardiology clinics*, vol. 25, pp. 141–70, vi, Feb. 2007. (Cited on page 4.)

[11] A. Kanitsar, D. Fleischmann, R. Wegenkittl, P. Felkel, and M. E. Gröller, "CPR - Curved Planar Reformation," in *IEEE Visualization Conf.*, pp. 37–44, 2002. (Cited on pages 4 and 61.)

[12] C. Slager, J. Wentzel, F. Gijsen, J. Schuurbiers, A. van der Wal, A. van der Steen, and P. Serruys, "The role of shear stress in the generation of rupture-prone vulnerable plaques," *Nature Clinical Practice Cardiovascular Medicine*, vol. 2, pp. 401–407, Aug. 2005. (Cited on page 5.)

[13] T. G. Papaioannou and C. Stefanadis, "Vascular Wall Shear Stress : Basic Principles and," *Hellenic J Cardiol*, vol. 46, pp. 9–15, 2005. (Cited on pages 5 and 49.)

[14] R. Torii, J. Keegan, N. B. Wood, A. W. Dowsey, A. D. Hughes, G.-Z. Yang, D. N. Firmin, S. A. Mcg Thom, and X. Y. Xu, "The effect of dynamic vessel motion on haemodynamic parameters in the right coronary artery: a combined MR and CFD study.," *The British journal of radiology*, vol. 82 Spec No, pp. S24–32, Jan. 2009. (Cited on pages 5, 19, 26, and 41.)

[15] C. Zhang, S. Xie, S. Li, F. Pu, X. Deng, Y. Fan, and D. Li, "Flow patterns and wall shear stress distribution in human internal carotid arteries: the geometric effect on the risk for stenoses.," *Journal of biomechanics*, vol. 45, pp. 83–9, Jan. 2012. (Cited on page 26.)

[16] X. Xie, Y. Wang, and H. Zhou, "Impact of coronary tortuosity on the coronary blood flow: A 3D computational study," *Journal of Biomechanics*, vol. 46, no. 11, pp. 1833–1841, 2013. (Cited on pages 5, 17, 19, 28, 29, and 41.)

[17] V. Peiffer, S. J. Sherwin, and P. D. Weinberg, "Does low and oscillatory wall shear stress correlate spatially with early atherosclerosis? A systematic review.," *Cardiovascular research*, vol. 99, pp. 242–50, July 2013. (Cited on pages 5, 16, and 41.)

[18] E. S. Weydahl and J. E. Moore, "Dynamic curvature strongly affects wall shear rates in a coronary artery bifurcation model.," *Journal of biomechanics*, vol. 34, pp. 1189–96, Sept. 2001. (Cited on page 5.)

[19] I. V. Pivkin, P. D. Richardson, D. H. Laidlaw, and G. E. Karniadakis, "Combined effects of pulsatile flow and dynamic curvature on wall shear stress in a coronary artery bifurcation model.," *Journal of biomechanics*, vol. 38, pp. 1283–90, June 2005. (Cited on pages 5, 19, and 41.)

[20] T. Iwami, T. Fujii, T. Miura, N. Otani, H. Iida, A. Kawamura, S. Yoshitake, M. Kohno, Y. Hisamatsu, H. Iwamoto, and M. Matsuzaki, "Importance of Left Anterior Descending Coronary Artery Curvature in Determining Cross-Sectional Plaque Distribution Assessed by Intravascular Ultrasound," *The American Journal of Cardiology*, vol. 82, pp. 381–384, 1998. (Cited on pages 5, 9, 19, and 41.)

[21] J. J. Wentzel, E. Janssen, J. Vos, J. C. H. Schuurbiers, R. Krams, P. W. Serruys, P. J. de Feyter, and C. J. Slager, "Extension of increased atherosclerotic wall thickness into high shear stress regions is associated with loss of compensatory remodeling.," *Circulation*, vol. 108, pp. 17–23, July 2003. (Cited on pages 9 and 16.)

[22] F. J. H. Gijsen, J. J. Wentzel, A. Thury, B. Lamers, J. C. H. Schuurbiers, P. W. Serruys, and A. F. van der Steen, "A new imaging technique to study 3-D plaque and shear stress distribution in human coronary artery bifurcations in vivo.," *Journal of biomechanics*, vol. 40, pp. 2349–57, Jan. 2007. (Cited on page 16.)

[23] C. M. Gibson, L. Diaz, K. Kandarpa, F. M. Sacks, R. C. Pasternak, T. Sandor, C. Feldman, and P. H. Stone, "Relation of vessel wall shear stress to atherosclerosis progression in human coronary arteries," *Arteriosclerosis, Thrombosis, and Vascular Biology*, vol. 13, pp. 310–315, Feb. 1993. (Cited on pages 9 and 16.)

[24] Y. Li, C. Shen, Y. Ji, Y. Feng, G. Ma, and N. Liu, "Clinical Implication of Coronary Tortuosity in Patients with Coronary Artery Disease," *PLoS One*, vol. 6, no. 8, pp. 1–5, 2011. (Cited on pages 9, 17, and 28.)

[25] M. A. M. Den Dekker, J. J. A. M. van den Dungen, I. F. J. Tielliu, R. A. Tio, M. M. J. J. R. Jaspers, M. Oudkerk, and R. Vliegenthart, "Prevalence of severe subclinical coronary artery disease on cardiac CT and MRI in patients with extra-cardiac arterial disease.," *European journal of vascular and endovascular surgery : the official journal of the European Society for Vascular Surgery*, vol. 46, pp. 680–9, Dec. 2013. (Cited on pages 10 and 40.)

[26] G. Rubin, D. Paik, P. Johnston, and S. Napel, "Measurement of the Aorta and Its Branches with Helical CT," *Radiology*, vol. 206, no. 3, pp. 823–9, 1998. (Cited on page 11.)

[27] J. C. Léger, "Menger curvature and rectifiability," *Annals of Mathematics*, vol. 149, pp. 831–869, 1999. (Cited on pages 11, 17, and 22.)

[28] E. L. Chaikof, M. F. Fillinger, J. S. Matsumura, R. B. Rutherford, G. H. White, J. D. Blankensteijn, V. M. Bernhard, P. L. Harris, K. Kent, J. May, F. J. Veith, and C. K. Zarins, "Identifying and grading factors that modify the outcome of endovascular aortic aneurysm repair," *Journal of Vascular Surgery*, vol. 35, pp. 1061–1066, May 2002. (Cited on pages 11 and 49.)

[29] J. R. Landis and G. G. Koch, "The Measurement of Observer Agreement for Categorical Data Data for Categorical of Observer Agreement The Measurement," *Biometrics*, vol. 33, pp. 159–174, 1977. (Cited on page 11.)

[30] R. Krams, J. J. Wentzel, and J. Oomen, "Evaluation of Endothelial Shear Stress and 3D Geometry as Factors Determining the Development of Atherosclerosis and Remodeling in Human Coronary Arteris in Vivo," *Arteriosclerosis, thrombosis, and vascular biology*, vol. 17, pp. 2061–2065, 1997. (Cited on page 16.)

[31] U. Olgac, V. Kurtcuoglu, S. C. Saur, and D. Poulikakos, "Identification of atherosclerotic lesion-prone sites through patient-specific simulation of low-density lipoprotein accumulation.," *Med Image Comput Comput Assist Interv*, vol. 11, no. Pt 2, pp. 774–81, 2008.

[32] Y. S. Chatzizisis, M. Jonas, A. U. Coskun, R. Beigel, B. V. Stone, C. Maynard, R. G. Gerrity, W. Daley, C. Rogers, E. R. Edelman, C. L. Feldman, and P. H. Stone, "Prediction of the localization of high-risk coronary atherosclerotic plaques on the basis of low endothelial shear stress: an intravascular ultrasound and histopathology natural history study.," *Circulation*, vol. 117, pp. 993–1002, Feb. 2008.

[33] K. C. Koskinas, C. L. Feldman, Y. S. Chatzizisis, A. U. Coskun, M. Jonas, C. Maynard, A. B. Baker, M. I. Papafaklis, E. R. Edelman, and P. H. Stone, "Natural history of experimental coronary atherosclerosis and vascular remodeling in relation to endothelial shear stress: a serial, in vivo intravascular ultrasound study.," *Circulation*, vol. 121, pp. 2092–101, May 2010. (Cited on page 16.)

[34] P. H. Stone, S. Saito, S. Takahashi, Y. Makita, S. Nakamura, T. Kawasaki, A. Takahashi, T. Katsuki, S. Nakamura, A. Namiki, A. Hirohata, T. Matsumura, S. Yamazaki, H. Yokoi, S. Tanaka, S. Otsuji, F. Yoshimachi, J. Honye, D. Harwood, M. Reitman, A. U. Coskun, M. I. Papafaklis, and C. L. Feldman, "Prediction of progression of coronary artery disease and clinical outcomes using vascular profiling of endothelial shear stress and arterial plaque characteristics: the PREDICTION Study.," *Circulation*, vol. 126, pp. 172–81, July 2012. (Cited on page 16.)

[35] N. Arora, M. E. Matheny, C. Sepke, and F. S. Resnic, "A propensity analysis of the risk of vascular complications after cardiac catheterization procedures with the use of vascular closure devices.," *American heart journal*, vol. 153, pp. 606–11, Apr. 2007. (Cited on page 16.)

[36] I. Springer and M. Dewey, "Comparison of multislice computed tomography with intravascular ultrasound for detection and characterization of coronary artery plaques: a systematic review.," *European journal of radiology*, vol. 71, pp. 275–82, Aug. 2009. (Cited on pages 16 and 19.)

[37] F. Pelliccia, V. Pasceri, A. Evangelista, A. Pergolini, F. Barillà, N. Viceconte, G. Tanzilli, M. Schiariti, C. Greco, and C. Gaudio, "Diagnostic accuracy of 320-row computed tomography as compared with invasive coronary angiography in unselected, consecutive patients with suspected coronary artery disease.," *The international journal of cardiovascular imaging*, vol. 29, pp. 443–52, Feb. 2013. (Cited on pages 16 and 19.)

[38] N. Dowson, M. Boult, P. Cowled, T. De Loryn, and R. Fitridge, "Development of an Automated Measure of Iliac Artery Tortuosity that Successfully Predicts Early Graft-Related Complications Associated with Endovascular Aneurysm Repair.," *European journal of vascular and endovascular surgery : the official journal of the European Society for Vascular Surgery*, vol. 48, pp. 153–60, Aug. 2014. (Cited on pages 17, 28, and 29.)

[39] T. Ghatwary, A. Karthikesalingam, B. Patterson, R. Hinchliffe, R. Morgan, I. Loftus, A. Salem, M. M. Thompson, and P. J. Holt, "St George ' s Vascular Institute Protocol: An Accurate and Reproducible Methodology to Enable Comprehensive Characterization of Infrarenal Abdominal Aortic Aneurysm Morphology in Clinical and Research Applications," *J Endovasc. Ther.*, vol. 19, pp. 400–414, 2012.

[40] T. R. Wyss, F. Dick, L. C. Brown, and R. M. Greenhalgh, "The influence of thrombus, calcification, angulation, and tortuosity of attachment sites on the time to the first graft-related complication after endovascular aneurysm repair.," *Journal of vascular surgery*, vol. 54, pp. 965–71, Oct. 2011. (Cited on pages 17 and 28.)

[41] Y. G. Wolf, M. Tillich, W. A. Lee, G. D. Rubin, T. J. Fogarty, and C. K. Zarins, "Impact of aortoiliac tortuosity on endovascular repair of abdominal aortic aneurysms: evaluation of 3D computer-based assessment.," *Journal of vascular surgery*, vol. 34, pp. 594–9, Oct. 2001. (Cited on page 17.)

[42] Y. Li, Z. Shi, Y. Cai, Y. Feng, G. Ma, C. Shen, and Z. Li, "Impact of Coronary Tortuosity on Coronary Pressure : Numerical Simulation Study," *PLoS One*, vol. 7, no. 8, pp. 3–8, 2012.

[43] O. Turgut, A. Yilmaz, K. Yalta, B. M. Yilmaz, A. Ozyol, O. Kendirlioglu, F. Karadas, and I. Tandogan, "Tortuosity of coronary arteries: an indicator for impaired left ventricular relaxation?," *The international journal of cardiovascular imaging*, vol. 23, pp. 671–7, Dec. 2007. (Cited on pages 17 and 28.)

[44] H. Zhu and M. H. Friedman, "Relationship between the dynamic geometry and wall thickness of a human coronary artery.," *Arteriosclerosis, thrombosis, and vascular biology*, vol. 23, pp. 2260–5, Dec. 2003. (Cited on pages 17 and 29.)

[45] H. Zhu, Z. Ding, R. N. Piana, T. R. Gehrig, and M. H. Friedman, "Cataloguing the geometry of the human coronary arteries: A potential tool for predicting risk of coronary artery disease," *International Journal of Cardiology*, vol. 135, no. 1, pp. 43–52, 2009. (Cited on pages 19 and 27.)

[46] M. Prosi, K. Perktold, Z. Ding, and M. H. Friedman, "Influence of curvature dynamics on pulsatile coronary artery flow in a realistic bifurcation model.," *Journal of biomechanics*, vol. 37, pp. 1767–75, Nov. 2004. (Cited on pages 19, 26, 29, and 41.)

[47] M. J. Johnson and G. Dougherty, "Robust measures of three-dimensional vascular tortuosity based on the minimum curvature of approximating polynomial spline fits to the vessel mid-line.," *Medical engineering & physics*, vol. 29, pp. 677–90, July 2007. (Cited on pages 19, 27, and 41.)

[48] P. M. O'Flynn, G. O'Sullivan, and A. S. Pandit, "Methods for three-dimensional geometric characterization of the arterial vasculature.," *Annals of biomedical engineering*, vol. 35, pp. 1368–81, Aug. 2007. (Cited on pages 17 and 29.)

[49] A. Theodorakakos, M. Gavaises, A. Andriotis, A. Zifan, P. Liatsis, I. Pantos, E. P. Efstathopoulos, and D. Katritsis, "Simulation of cardiac motion on non-Newtonian, pulsating flow development in the human left anterior descending coronary artery.," *Physics in medicine and biology*, vol. 53, pp. 4875–92, Sept. 2008. (Cited on pages 19 and 41.)

[50] D. Zeng, Z. Ding, M. H. Friedman, and C. R. Ethier, "Effects of Cardiac Motion on Right Coronary Artery Hemodynamics," *Annals of Biomedical Engineering*, vol. 31, pp. 420–429, Apr. 2003. (Cited on pages 19, 26, and 41.)

[51] A. J. O'Loughlin, S. Kazi, J. K. French, D. A. B. Richards, A. R. Denniss, and A. Hennessy, "Quantitative Coronary Artery Motion Analysis Predicts the Location of Future ST Segment Elevation Myocardial Infarctions," *International journal of cardiovascular and cerebrovascular disease*, vol. 2, no. 3, pp. 35–38, 2014. (Cited on page 19.)

[52] A. J. O'Loughlin, L. Tang, D. Moses, W. T. Diagrad, J. K. French, and D. Ab, "A Novel Quantitative Index of Coronary Artery Motion from Multislice Computed Tomography and the Location of Coronary Artery Disease," *International journal of cardiovascular and cerebrovascular disease*, vol. 2, no. 1, pp. 1–5, 2014. (Cited on pages 19 and 28.)

[53] L. H. Piers, R. Dikkers, T. P. Willems, B. J. G. L. de Smet, M. Oudkerk, F. Zijlstra, and R. A. Tio, "Computed tomographic angiography or conventional coronary angiography in therapeutic decision-making.," *European heart journal*, vol. 29, pp. 2902–7, Dec. 2008. (Cited on pages 20, 26, 31, 40, 49, and 66.)

[54] A. M. de Vos, A. Rutten, H. J. van de Zaag-Loonen, M. L. Bots, R. Dikkers, R. A. Buiskool, W. P. Mali, D. D. Lubbers, A. Mosterd, M. Prokop, B. J. Rensing, M. J. Cramer, H. W. van Es, F. L. Moll, E. D. van de Pavoordt, P. A. Doevendans, B. K. Velthuis, A. J. Mackaay, F. Zijlstra, and M. Oudkerk, "Non-invasive cardiac assessment in high risk patients (The GROUND study): rationale, objectives and design of a multi-center randomized controlled clinical trial.," *Trials*, vol. 9, p. 49, Jan. 2008. (Cited on pages 20 and 40.)

[55] H. M. Willemsen, G. de Jong, R. A. Tio, W. Nieuwland, I. P. Kema, I. C. C. van der Horst, M. Oudkerk, and F. Zijlstra, "Quick identification of acute chest pain patients study (QICS).," *BMC cardiovascular disorders*, vol. 9, p. 24, Jan. 2009. (Cited on pages 20, 31, and 40.)

[56] H. J. Kim, I. E. Vignon-Clementel, J. S. Coogan, C. A. Figueroa, K. E. Jansen, and C. A. Taylor, "Patient-specific modeling of blood flow and pressure in human coronary arteries.," *Annals of biomedical engineering*, vol. 38, pp. 3195–209, Oct. 2010. (Cited on page 27.)

[57] K. U. Juergens, M. Grude, D. Maintz, E. M. Fallenberg, T. Wichter, W. Heindel, and R. Fischbach, "Multi-detector row CT of left ventricular function with dedicated analysis software versus MR imaging: initial experience.," *Radiology*, vol. 230, pp. 403–10, Feb. 2004. (Cited on page 27.)

[58] D. L. Brutsaert, "Cardiac endothelial-myocardial signaling: its role in cardiac growth, contractile performance, and rhythmicity.," *Physiological reviews*, vol. 83, pp. 59–115, Jan. 2003. (Cited on page 28.)

[59] T. Konta, J. Hugh, and N. Bett, "Patterns of Coronary Artery Movement and the Development of Coronary Atherosclerosis," *Circ J*, vol. 67, no. October, pp. 846–850, 2003. (Cited on pages 28 and 31.)

[60] S. S. Groves and B. E. Warden, "Severe coronary tortuosity and the relationship to significant coronary artery disease," *West Virginia Medical Journal*, vol. 105, no. 4, pp. 14–17, 2009. (Cited on page 28.)

[61] B. M. Johnston and P. R. Johnston, "The relative effects of arterial curvature and lumen diameter on wall shear stress distributions in human right coronary arteries.," *Physics in medicine and biology*, vol. 52, pp. 2531–44, May 2007. (Cited on page 29.)

[62] O. Smedby, N. Högman, S. Nilsson, U. Erikson, A. G. Olsson, and G. Walldius, "Two-Dimensional Tortuosity of the Superficial Femoral Artery in Early Atherosclerosis," *Journal of Vascular Research*, vol. 30, no. 4, pp. 181–191, 1993. (Cited on page 29.)

[63] E. Bullitt, G. Gerig, S. M. Pizer, W. Lin, and S. R. Aylward, "Measuring Tortuosity of the Intracerebral Vasculature from MRA Images," *IEEE Trans Med Imaging*, vol. 22, no. 9, pp. 1163–1171, 2003. (Cited on page 29.)

[64] M. Schaap, C. T. Metz, T. van Walsum, A. G. van der Giessen, A. C. Weustink, N. R. Mollet, C. Bauer, H. Bogunović, C. Castro, X. Deng, E. Dikici, T. O'Donnell, M. Frenay, O. Friman, M. Hernández Hoyos, P. H. Kitslaar, K. Krissian, C. Kühnel, M. A. Luengo-Oroz, M. Orkisz, O. Smedby, M. Styner, A. Szymczak, H. Tek, C. Wang, S. K. Warfield, S. Zambal, Y. Zhang, G. P. Krestin, and W. J. Niessen, "Standardized evaluation methodology and reference database for evaluating coronary artery centerline extraction algorithms.," *Medical image analysis*, vol. 13, pp. 701–14, Oct. 2009. (Cited on pages 41 and 46.)

[65] A. V. Finn, Y. Chandrashekhar, and J. Narula, "IVUS and OCT: either or survivor ....," *JACC. Cardiovascular imaging*, vol. 4, pp. 1047–9, Sept. 2011. (Cited on page 41.)

[66] W. J. Stuijfzand, I. Danad, P. G. Raijmakers, C. B. Marcu, M. W. Heymans, C. C. van Kuijk, A. C. van Rossum, K. Nieman, J. K. Min, J. Leipsic, N. van Royen, and P. Knaapen, "Additional Value of Transluminal Attenuation Gradient in CT Angiography to Predict Hemodynamic Significance of Coronary Artery Stenosis.," *JACC. Cardiovascular imaging*, vol. 7, pp. 374–86, Apr. 2014. (Cited on page 42.)

[67] B. Lu, S.-S. Mao, N. Zhuang, H. Bakhsheshi, H. Yamamoto, J. Takasu, S. C. K. Liu, and M. J. Budoff, "Coronary Artery Motion During the Cardiac Cycle and Optimal ECG Triggering for Coronary Artery Imaging," *Investigative Radiology*, vol. 36, pp. 250–256, May 2001. (Cited on page 44.)

[68] J.-L. Sablayrolles and P. Giat, "Visualization Techniques for Contrast-Enhanced CT Angiography of Coronary Arteries," in *CT of the Heart SE - 24* (U. Schoepf, ed.), Contemporary Cardiology, pp. 247–258, Humana Press, 2005. (Cited on page 47.)

[69] C. Fink, R. Krissak, T. Henzler, U. Lechel, G. Brix, R. A. P. Takx, J. W. Nance, J. A. Abro, S. O. Schoenberg, and U. J. Schoepf, "Radiation dose at coronary CT angiography: second-generation dual-source CT versus single-source 64-MDCT and first-generation dual-source CT.," *AJR. American journal of roentgenology*, vol. 196, pp. W550–7, May 2011. (Cited on pages 49 and 66.)

[70] G. Dougherty and J. Varro, "A quantitative index for the measurement of the tortuosity of blood vessels," *Medical Engineering & Physics*, vol. 22, no. 2000, pp. 567–574, 2001. (Cited on page 49.)

List of Abbreviations

AHA American Heart Association

AV atrioventricular

CFD computational fluid dynamics

CPR curved planar reformation

DSCT dual-source computed tomography

ECG electrocardiography

ED end diastole

ES end systole

ICC intraclass correlation coefficient

IVUS intravascular ultrasound

LAD left anterior descending

LCX left circumflex

LM left main

MDCT multi-detector computed tomography

MR magnetic resonance

PDA posterior descending artery

RCA right coronary artery

UMCG University Medical Center Groningen

WSS wall shear stress

List of Figures

List of Tables

Dankwoord

Na een jaar te hebben gewerkt aan mijn afstudeeronderzoek is het einde hiervan in zicht en zal ik hiermee een 6-jarige periode van studeren achter me laten. In deze jaren en zeker ook het laatste jaar, heb ik veel gehad aan een groot aantal personen waar ik wekelijks of dagelijks mee om ben gegaan. Graag wil ik hen hier bedanken.

Beste Peter en Rozemarijn, van jullie heb ik ontzettend veel kunnen leren! Niet alleen inhoudelijk op cardiovasculair gebied en de bijbehorende kliniek/imaging, maar vooral ook als academicus. Daarnaast weet ik zeker dat jullie vele feedback mij als persoon bewuster heeft gemaakt van mijn eigen (on)mogelijkheden en eigenschappen. Vooral voor de kansen die jullie me hebben gegeven om me ontwikkelen tijdens mijn afstuderen in Groningen (en eventueel daarna samen met prof. Oudkerk) wil ik jullie enorm bedanken.

Ook professor Slump wil ik hierbij graag bedanken, als technisch begeleider tijdens meerdere stages. Het was qua afstand nog wel eens lastig om elkaar regelmatig te spreken, maar als we een bespreking of feedbackmoment hebben gehad, stond ik toch telkens achteraf versteld van hoeveel bruikbare informatie of aanknopingspunten het me had opgeleverd. Op dergelijke momenten zal ik altijd blijven hopen. Paul van Katwijk, al vanaf het eerste jaar van mijn opleiding ben jij betrokken geweest. Achteraf moet ik zeker zeggen dat de discussies tijdens intervisie en de vele reflecties toch vaak een aangename eye-opener voor me zijn geweest. Ook Bernhard van Driel wil ik bij deze graag bedanken, en niet in de laatste plaats voor zijn legio ervaringen en 'trucjes' om een onderscheid te kunnen maken in een medisch-technische wereld.

Natuurlijk de collega's van de G2-afdeling voor de talloze gezellige lunches, borrels, koffiepauzes, en researchclub momenten. Stella, voor het verloop van mijn stage en de extra ervaringen die ik hierin heb op kunnen doen wil ik jou ook graag bedanken. Beste Volkan, na onze samenwerking hoop ik je ooit nog eens terug te zien in Nederland. Last but not least van de G2, Wout en Gert Jan. Jullie 'extra-curriculaire' inspiraties die ik niet allemaal zal benoemen hebben mij zeker voor een groot deel door deze laatste stage geloodst! In het UMCG heb ik verder veel contact gehad met een grote groep medisch professionals, die ik graag allemaal hartelijk wil bedanken voor alle (klinische) ervaringen en het dagelijkse onderwijs.

Een laatste alinea is natuurlijk bestemd voor mijn familie. Ik wil jullie graag heel erg bedanken voor alle momenten waarin jullie mij een hart onder de riem hebben gestoken en in meer of mindere mate betrokken zijn geweest bij wat en waar ik dat deed. Papa en mama, zonder jullie onvoorwaardelijke hulp en liefde had ik deze 6 jaren niet kunnen volbrengen!

Lieve Marlot, op jou kan ik altijd rekenen. Nu we eindelijk geen student meer zijn, ga ik graag met jou een zonnige toekomst tegemoet!

APPENDIX A

Additional Figures

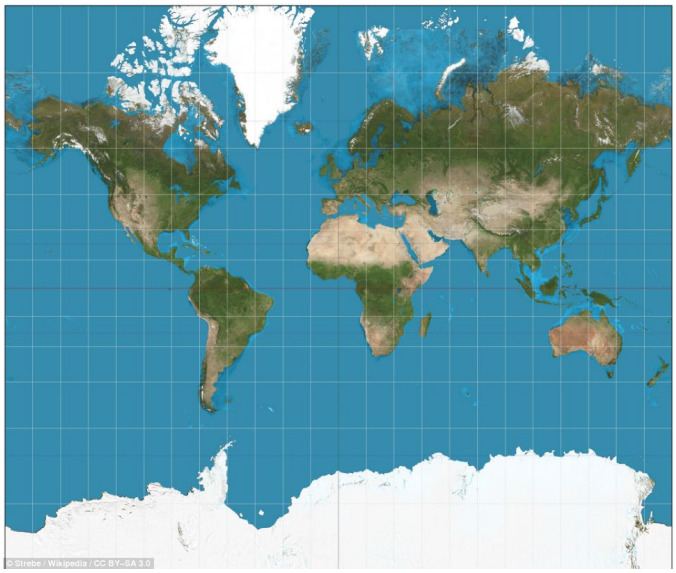

Figure A.1: Mercator projection of the earth's surface. Greenland and Antarctica for example are deformed and unduly magnified, because of transforming spherical information into a flat image. Analogous situation to the 'projected' CPR distortions of tissue not located at the centerline. From http://tinyurl.com/q554h4v.

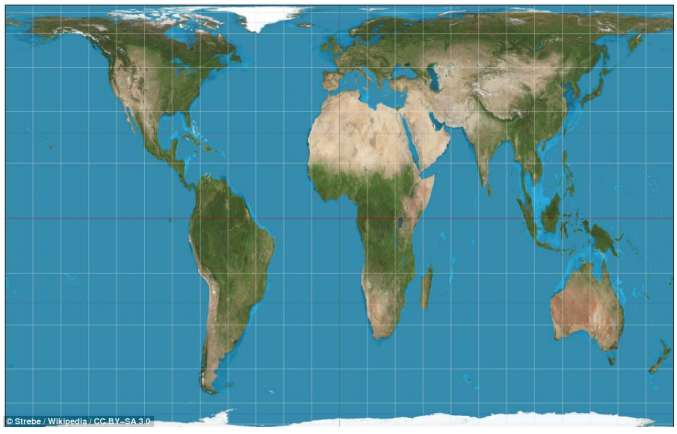

Figure A.2: Alternative projection of the earth's surface. Although the land size is now correct, land at the poles (horizontally stretched) and Equator (vertically stretched) is still deformed, which also happens to tissue with 'stretched' CPR. From http://tinyurl.com/q554h4v.

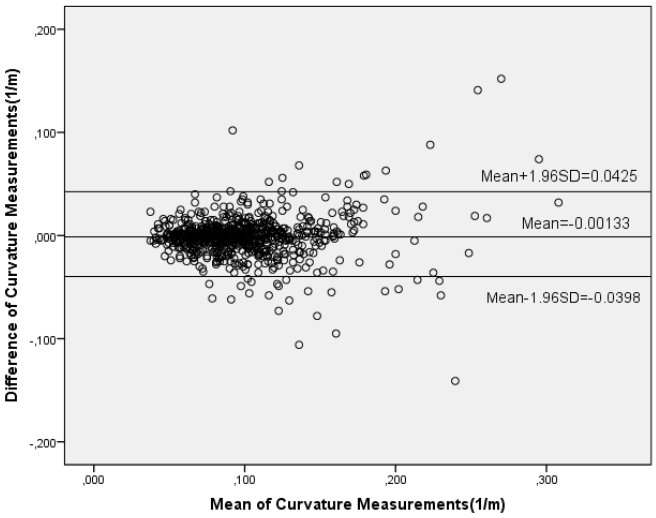

Figure A.3: Bland-Altman plots for intra-reader differences of curvature measurements in the patient group from Chapter 2.

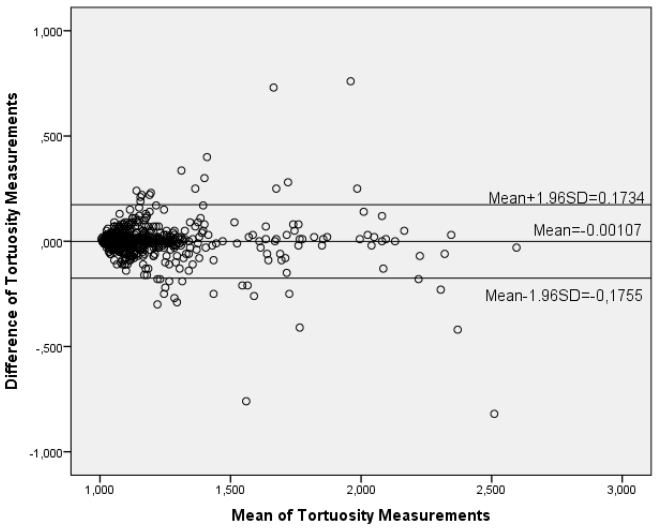

Figure A.4: Bland-Altman plots for intra-reader differences of tortuosity measurements in the patient group from Chapter 2.

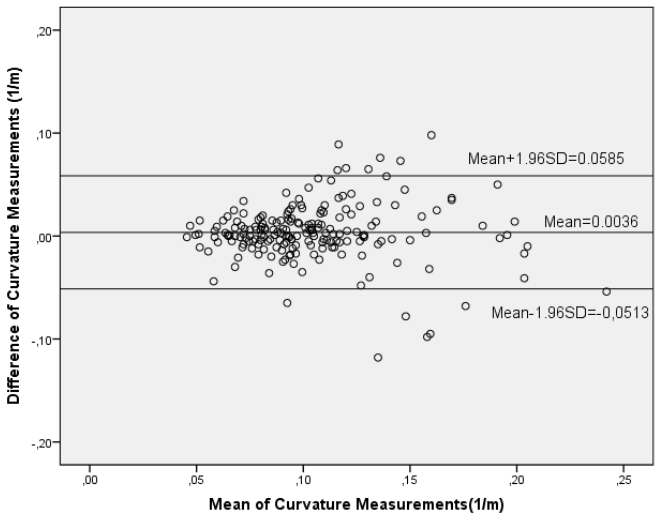

Figure A.5: Bland-Altman plots for inter-reader differences of curvature measurements in the patient group from Chapter 2.

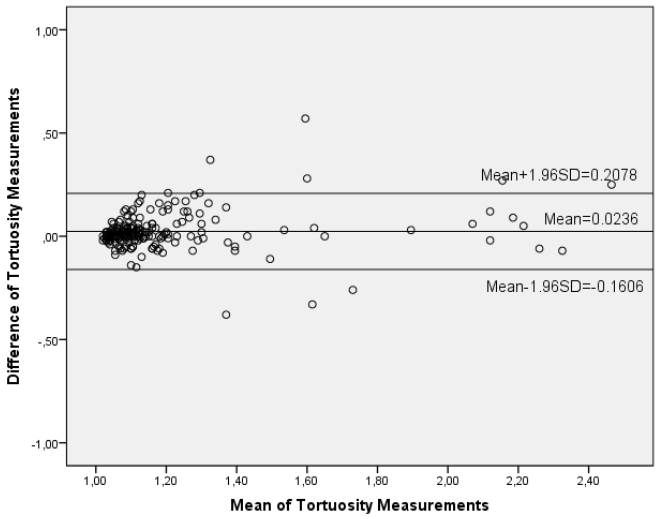

Figure A.6: Bland-Altman plots for inter-reader differences of tortuosity measurements in the patient group from Chapter 2.